Decoding Sequence-Structure-Function-Evolution of basic Leucine Zippers of Aureochromes from Heterokont Algae

Madhurima Khamaru[a], Debarshi Bose[a], Anwesha Deb[a] and Devrani Mitra[a*]

[a]Department of Life Sciences, Presidency University, 86/1 College Street, Kolkata – 700073, WB, India

[*]Address of correspondence - devrani.dbs@presiuniv.ac.in

Running title – Decoding bZIPs: Aureochromes versus the Rest

Keywords

Aureochrome; Basic leucine zipper; Protein-DNA interaction; Phylogeny and (co)evolution; Electrophoretic mobility shift assay (EMSA), Molecular Dynamics Simulation, All-atom network, Photosynthetic stramenopiles, *Ectocarpus siliculosus*, Optogenetics

Highlights

- Aureochrome is perhaps the only light-responsive transcription factor in bZIP superfamily.
- We draw a comparative between aureochromes and other bZIPs via *in-silico*/*in-vitro* methods.
- Aureochromes form a distinctly separate lineage, midway in bZIP evolution.
- The unique histidine facilitates aureochromes' interaction with cognate DNA substrates.

Abstract

The blue light photoreceptor cum transcription factors, Aureochromes (Aureos), are present exclusively in photosynthetic stramenopiles. Co-existence of Light-Oxygen-Voltage (LOV) and basic leucine zipper (bZIP) is unique to Aureos – therefore ideal to study light-dependent DNA binding/transcriptional regulation. Further, Aureos' inverse effector-sensor topology, resembling several sensory eukaryotic transcription factors, makes them prototypical optogenetic scaffolds. In absence of 3D data, this study aims for a thorough investigation of

the bZIP domains from Aureos and others, and their interaction with substrate DNA using tools from sequence/structural bioinformatics, network theory, molecular dynamics simulation and *in vitro* experiments. An in-depth comparison of 173 Aureo/plant/opisthokont bZIPs reveals Aureos' uniqueness and evolutionary significance in DNA binding specificity as well as dimer stability. An all-atom network analysis on representative bZIP-DNA co-crystal structures, especially the measurement of eigenvector centrality, further adds importance to hydrophobic interactions in the zipper region to stabilize bZIP dimer and facilitate DNA binding in Aureos and other bZIPs. Perhaps the most notable finding is the unique histidine substitution at the basic region of Aureos unlike any other bZIPs. Not only is this residue important for DNA binding, this can serve as a potential switch point in Aureo/bZIP evolution.

1. Introduction

Regulation of gene expression is essential for the survival of every life form. Transcription factors (TFs), upon binding with the cognate DNA, turn genes on/off at precise spatio-temporal resolution. Different classes of transcription factors exist. They differ on the basis of their DNA binding structural motifs and activity. Examples include basic leucine zipper (bZIP), basic helix-loop-helix (bHLH), Zinc-coordinating DNA-binding motifs (Zinc finger), helix-turn-helix (HTH), beta scaffold factors like STAT (Signal transducer and activator of transcription proteins), MADS (MCM1, AGAMOUS, DEFICIENS, and SRF) box, HMG box (high mobility group box), TBP (TATA-binding protein), Beta barrel alpha helix etc. Among these, bZIPs comprise one of the largest group of eukaryotic transcription factors (Ji et al., 2018). The uniqueness of bZIPs lies in their conserved nature of structure and sequence specificity. They possess N-X7-R/K signature motif and binds mostly to the *cis* acting DNA elements of a promoter having an 'ACGT' core sequence (Wang et al., 2018) (Rodríguez-Martínez et al., 2017). Interdigitation between the partner helices leads to the dimerization of bZIP — resulting in a superimposed coiled coil structure or 'zipper' (Bader & Vogt, 2006)(Sinden, 1994). This zipper-like structure is extended by the N-terminal helical segment, which can bind to the DNA major groove via basic amino acid residues(Glover & Harrison, 1995). Dimerization is essential for the recognition of substrate DNA and transcriptional regulation. The C-terminal zipper motif consists of heptads, which can be represented by a helical wheel. The residues are conventionally marked from 'a' to 'g' (Grigoryan & Keating, 2006), where leucines generally occupy every 'd' position, whereas the hydrophobic residues including leucine/isoleucine dominate 'a' (Bader & Vogt, 2006).

However, presence of a conserved asparagine at ‘a’ position in the middle of zipper could result in destabilization of the oligomer (Harbury et al., 1993). The ‘b’, ‘c’ and ‘f’ positions are generally filled by polar residues. The charged residues at the ‘e’ and ‘g’ positions also aid in the zipper dimer stability (Deppmann et al., 2004)(Podust et al., 2001). Leucine residues, owing to their hydrophobic side chains, create ‘knobs’ which can fit into the ‘holes’ generated in between the side chains of amino acids present in adjacent helices (Bader & Vogt, 2006). At the other end, the basic amino acid residues complement well with the negatively charged phosphate backbone of DNA — this results in favorable electrostatic interactions. Besides, they can also participate in hydrogen bonding/polar interactions and can even engage in non-polar interactions with the portions of extended side chains. Besides phosphates, the nitrogenous base and deoxyribose sugar are also involved in hydrogen bonding, van der Waal’s as well as stacking interactions. The affinity of bZIP TFs towards the cognate target DNA sequences is imparted by the sequence composition of its basic region as well as the length of the leucine zipper (Hakoshima, 2005a). The dimerization partner is also crucial for its sequence specific DNA binding (Pogenberg et al., 2014). Their ability to bring in change in the binding specificity upon hetero-dimerization is indicative of this (Busch & Sassone-Corsi, 1990). The electrostatic attraction and repulsion forces, acting between the polar residues that flank the hydrophobic interaction surface of the zippers, are major deciding factors behind the formation of homo/heterodimers (C. R. Vinson et al., 1993). The oppositely charged residues located at 'g' and the following e' positions across the hydrophobic interface, form the inter-helical ion bridges. The interactions between d-d', a-a', g-e' are vital for the zipper formation and stabilization (Podust et al., 2001).

Widespread among the regulatory proteins of gene expression, the bZIPs play a crucial role in cellular proliferation and differentiation in eukaryotes. It is known to be the ancient DNA binding module found across three kingdoms of life (Hakoshima, 2005b). Several groups of opisthokont and plant bZIPs are well defined and characterized. Few homologs of bZIPs are also evident in fungi, algae, protists and even in bacteria. However, the only blue light (BL) responsive photoreceptor with a bZIP TF activity has been recently discovered (Takahashi et al., 2007) in Aureos – found exclusively in photosynthetic stramenopiles (Rayko et al., 2010). The flavin binding Light-Oxygen-Voltage (LOV) BL sensor at the C-terminus, makes Aureos different from any other conventional bZIPs. Aureos perform organism specific diverse functionalities [**SI-1**] e.g. - branching in *Vaucheria sp* (Takahashi et al., 2007), cell cycle progression in *Phaeodactylum sp* (Kroth et al., 2017),

lipid accumulation in *Nannochloropsis sp.* (Huang et al., 2014) etc. The broad spectrum functions of Aureos include promotion of high light acclimation, photo protection in diatoms etc (Huysman et al., 2013). Considering maximum penetration of BL in sea water, most of the physiological and developmental responses are BL dependent in photosynthetic marine algae. However, it lacks phototropins (Rayko et al., 2010), which is one of the major BL photoreceptors in land plants. Aureos instead aid in the optimization of photosynthesis (Mann et al., 2020) under varied light conditions. In fact, Aureos' significance in carrying out BL-mediated gene expression is not only important to study BL signaling in photosynthetic marine algae, they are potentially relevant for optogenetics as well. The direct DNA binding ability of Aureo in response to BL without an intricate signaling mechanism makes Aureo an ideal optogenetic scaffold. They are capable of bringing in faster changes in gene expression under fluctuating light conditions (Mann et al., 2020). Dual presence of a LOV photoreceptor and a bZIP TF domain empowers Aureo to serve as a natural optogenetic tool (Hepp, Trauth, Hasenjäger, et al., 2020) (Duan et al., 2018) (Jerng et al., 2021). In contrary to commonly-sighted domain topology in most LOV photoreceptors, the inverse effector-sensor arrangement in all Aureo is similar to that in several eukaryotic TFs (Matiiv & Chekunova, 2018) — a feature suitable for developing synthetic sensory TFs (Boral et al., 2022) as well as optogenetic designs (S. Banerjee & Mitra, 2020). While a substantial amount of literature is available against Aureo LOV sensors especially on their sequence-structure-function (Mitra et al., 2012) (A. Banerjee, Herman, Kottke, et al., 2016) (Hepp, Trauth, Hasenj, et al., 2020) (Heintz & Schlichting, 2016), structure based mechanistic insights is lacking for the effector bZIPs. And till date, no experimental structure corresponding to full-length or even the bZIP-linker-LOV module of Aureo is available in PDB. Therefore, a comprehensive sequence-structure characterization of this effector bZIP is attempted using several *in-silico* tools e.g. for phylogenetic studies, network theory, modelling, docking and molecular dynamics (MD) simulation to understand the formers' uniqueness and significance. We include all available varieties of Aureo_bZIPs and compare them with other traditional bZIP TFs found across plants and opisthokonts to understand the uniqueness and evolutionary significance. We further validate our *in-silico* results and assess the DNA binding ability of Aureo_bZIPs using *in-vitro* electrophoretic mobility shift assay (EMSA) after cloning, overexpression and protein purification. In this study, we attempt to draw an effective comparative between the bZIP domains of Aureos and the rest *via* a holistic sequence-structure-function characterization.

127 ## 2. Materials and Methods

128 ***2.1. Retrieval of bZIP sequences from different organisms*:** The amino acid sequences of
129 Aureos and other representative bZIP proteins from plants and opisthokonts were collected
130 from the UniProt (Apweiler et al., 2018) protein sequence database. BLASTP (Altschul et al.,
131 1990) search was also performed against the database of non-redundant protein sequences
132 using available bZIP sequences as queries. A few sequences, especially those of Aureos from
133 *Phaeodactylum sp*. were obtained from the available literature (Costa et al., 2013). Amino
134 acid sequences of the 78 bZIP proteins from plants, 69 bZIPs from opisthokont species and
135 26 Aureo bZIP sequences were shortlisted for further analyses. The respective domain
136 boundaries of the bZIPs were finalized either from 'conserved domain' analysis of NCBI and
137 Pfam, or from PSI-BLAST or domain BLAST of NCBI.

138 ***2.2 Sequence comparison and molecular evolutionary analysis*:** A total of 173 bZIP
139 sequences thus retrieved, were subjected to multiple sequence alignment using Clustal omega
140 (Sievers et al., 2011) algorithm — first group-wise and then collectively. This gave us a
141 preliminary understanding on the subtle differences in bZIP sequences that could lead to
142 differences in DNA binding activity. The sequences were further considered for the
143 construction of a phylogenetic tree using MEGA X programme (Kumar et al., 2018). The
144 corresponding accession numbers of all the database entries of these bZIP proteins along with
145 the names and source organisms are listed in the table (**SI-2**). For molecular evolutionary
146 analysis, all 173 bZIP sequences were first aligned using MUSCLE algorithm, inbuilt in
147 MEGA X. The most rational tree of all the selected bZIP proteins was drawn using the
148 neighbor joining (NJ) method, which is simple and fast. Poisson model, which considers
149 equality of substitution rates among all the sites and assumes equal frequencies of amino
150 acids at the time of correction of the multiple substitutions at the same sites, was followed as
151 the substitution method. The phylogeny was tested through bootstrap analysis where the
152 number of performances of bootstrap replications for each node was kept at 1000. The
153 redundant and partial sequences were discarded. Only the reviewed and annotated sequences
154 were considered. The guide tree was then represented and labeled by the online phylogenetic
155 tree manipulation tool iTOLv5. The clades in red and green represent the maximum and
156 minimum values of bootstrap respectively. A covariance analysis on Aureo bZIPs were
157 further performed using the GREMLIN (Kamisetty et al., 2013) server. Default parameters
158 like 4 iterations, >75% query coverage and 10^{-10} /10^{-4} E-value cut-off were chosen as
159 appropriate for this study.

160 ***2.3 Residue Interaction Graphs to understand bZIP-DNA interactions*:** The protein-DNA
161 complex structure can be represented as residue interaction graph (RIG) or an all-atom
162 network, where nodes (amino acids/nucleotide residues) are linked by edges within a given
163 distance cut off (e.g. 4.5 Å). To investigate further on the bZIP-DNA complexes, RIGs were
164 first generated from eight representative homo/heterodimeric bZIP co-crystal structures from
165 all the bZIP subfamilies, using the Biographs module of Biopython (Cock et al., 2009) and
166 NetworkX (Hagberg et al., 2008). Eight structures representing different bZIP subgroups are
167 - 2WTY (MAF), 1JNM (JUN-CRE complex), 1GD2 (PAP), 1YSA (GCN4), 1FOS (JUN-
168 FOS heterodimer), 1NWQ (CEBP), 1DH3 (CREB) and 2H7H (JUN-AP1 complex). The
169 RIGs were generated considering all atom-pair contacts within a given distance of 4.5 Å.
170 Centrality measures as simple as degree centrality, geodesic/shortest path based closeness
171 and betweenness centrality have been extremely helpful to identify influential nodes from
172 residue-level interaction data (Deb et al., 2020). However, to capture all communication at
173 the residue level, we calculated eigenvector centrality (EC) of the constructed RIGs. How
174 well connected a node is, in terms of its connectivity with other well-connected nodes of a
175 network, can be measured by EC. The weighted sum of the centralities of all nodes, which
176 are connected to node *'i'* by an edge *'A_{ij}'*, is defined as EC of node *'i'* (C_i) (Negre et al.,
177 2018)- $C_i = \varepsilon^{-1}\sum_{j=1}^{n} A_{ij}c_j$, where 'c' denotes the eigenvector associated with eigenvalue ε
178 of 'A'.

179 The distribution of EC was plotted next. We studied the value of Z (X) = (X-<X>)/σ, where
180 <X> and σ represent mean and standard deviation respectively. For subsequent analysis, we
181 therefore considered only those values of X which are associated with Z (X) > 1.5.

182 ***2.4 Modeling and docking of Aureo bZIPs - comparison with other bZIPs*:** Till date, no
183 experimental 3D structure corresponding to the bZIP region of Aureo is available in RCSB
184 PDB. Hence, the bZIP sequences, representatives from all five subtypes of Aureos sourced
185 from *Ectocarpus/Saccharina* sp, were individually modeled using SWISS-MODEL
186 (Waterhouse et al., 2018). The best models, selected on the basis of best Ramachandran
187 parameters, were next energy minimized using Chimera (Pettersen et al., 2004). The energy
188 minimized structures were next subjected to molecular docking analysis using NPDock
189 (Tuszynska et al., 2015). Review of literature suggests that the bZIP domain of Aureo binds
190 to a consensus DNA sequence TGACGT, named 'Aureo-box'(Matiiv & Chekunova, 2018)
191 (Takahashi et al., 2007). So, for the *in silico* docking of modeled Aureo_bZIPs with DNA,
192 'Aureo-box'(TGACGT) containing CRE (cAMP responsive element) DNA (A. Banerjee,

193 Herman, Kottke, et al., 2016) from co-crystal structure of CREB bZIP-CRE DNA [(PDB ID:
194 1DH3, (Schumacher et al., 2000) was used as the DNA substrate /ligand. Preliminary
195 knowledge on protein-DNA interaction interface, as acquired from sequence-structure
196 superposition with solved bZIP-DNA co-crystal structures and residue interaction graphs was
197 used as input in docking. The energy parameters, interface interactions as well as buried
198 surface area on the best scoring structures of Aureo_bZIP-DNA complexes were calculated
199 using PDBePISA (Evgeny, 2010). In order to perform a detailed comparative study between
200 aureochromes and the rest bZIPs, the hydrogen bonding and polar interactions at the basic
201 region of bZIP-DNA interfaces of all were analyzed using Chimera (Pettersen et al., 2004)
202 and Pymol (Delano, 2002). *In silico* mutagenesis was performed in few docked structures to
203 understand the functional as well as evolutionary significance of N-terminal basic region
204 residues of Aureo_bZIPs.

205 ***2.5 System Setup, Molecular Dynamics Simulations and Post-Simulation Methodologies:***
206 Following phylogeny and docking analyses, unique placement of histidine was noticed
207 exclusively at the basic region of Aureos and not in others. In order to investigate the specific
208 contribution of this residue in DNA binding activity, Molecular Dynamics (MD) Simulations
209 were performed using the GROMACS (version 2020.1) (Pronk et al., 2013) (Van Der Spoel
210 et al., 2005). The docked structure of *Ectocarpus siliculosus* Aureo1_bZIP-DNA complex
211 (*Es*Aureo1_wild) and its *in-silico* mutant versions (*Es*Aureo1_HA and *Es*Aureo1_HS) were
212 considered as initial files for MD simulation. AMBER99SB-ILDN force field was applied.
213 The docked bZIP-DNA complex was solvated using TIP3P water molecules and was limited
214 into a cubic lattice of dimensions 1.2 x 1.2 x 1.2 nm^3. The structures had positive charges at
215 normal physiological pH conditions, thus the addition of chloride (Cl^-) ions ensured the
216 simulation systems' electrical neutrality. The entire molecular structure was then relaxed by
217 performing energy minimization, starting with the steepest descent and followed by the
218 conjugate gradient algorithm. To remove the solute-solute and solute-solvent steric clashes
219 and allow the system to adapt to its environment stably, a harmonic restraint was imposed on
220 the solute particles keeping the solvent particles unrestrained, for over 50000 energy
221 minimisation steps for both algorithms. Before moving forward, the potential energy (E_{pot}) of
222 the system was checked to be a negative value, since it is correlated with the sufficient
223 stability of the system required for simulation. The equilibration process was conducted in
224 two steps. First, the isothermal-isochoric or NVT (constant number of particles-volume-
225 temperature) ensemble, followed by an isothermal-isobaric or NPT (constant number of

226 particles-pressure-temperature) ensemble was conducted for 100 ps each, with position
227 restraining for the non-water residues and constraints of the H-bonds. A leapfrog integrator
228 was used to analyze the dynamic system numerically. The Berendsen thermostat algorithm
229 was used for re-scaling the particle velocities in the simulation model to relax the system and
230 regulate the temperature inside the box to be at around 300 K. The Particle Mesh Ewald
231 (PME) method was utilized for rapid stochastic relaxation of the system to equilibrium and to
232 calculate long-range electrostatics. The pressure fluctuation of the simulation system was
233 accounted for by running an average over the entire length, which was compared with the
234 reference pressure set as 1 bar and an isothermal compressibility allowance of 4.5 x 10-5
235 bar^{-1} for water. The LINCS (LINear Constraint Solver) algorithm was used for bond
236 (involving hydrogens) restraining. An integration time step of 2 fs was applied and the log
237 file/ coordinate update was done every 1 ps. The system, thus prepared, was finally exposed
238 to the subsequent forces and ran for 60 ns (20 ns at a stretch for 3 consecutive times), at 300
239 K temperature.
240 The data obtained post-simulation (as .xvg files) were plotted using the XMGRACE plotting
241 tool. PyMOL (Delano, 2002) software was used for visual assessment of the bZIP-DNA
242 complexes during the simulatory period. The GROMACS in-built analysis package (Van Der
243 Spoel et al., 2005) was extensively utilized to elucidate all the analytical data for 60 ns MD
244 simulation run, which were compared for the wild-type and the mutant variants.
245 ***2.6 Cloning of wild type Aureochrome-1 from Ectocarpus siliculosus:*** The pUC-57
246 plasmids harboring the codon optimized synthetic gene corresponding to *Ectocarpus*
247 *siliculosus* aureochrome1 (*Es*Aureo1; Uniprot accession no.- D7FMH8) was purchased. PCR
248 amplification of the bZIP-linker-LOV sequence of wild type *Es*Aureo1 (*Es*Aureo1_Wild)
249 DNA sequence was carried out using the following forward primer (FP) and reverse primer
250 (RP) respectively-5'CTAGGCTAGCATGAAAGATCTGACCGAAGAACAGCGCATTG3';
251 5'AGCTGAGCTCTTATTTGCTCGGGCCCGCCAGCTG3'. The *Es*Aureo1_wild was then
252 cloned into the pET28a expression vector at the NheI/SacI restriction sites.
253 ***2.7 Site directed mutagenesis:*** To uncover the role of unique histidine substitution at the
254 basic region of Aureos, His362 residue in *Es*Aureo1_wild was next mutated to alanine and
255 serine. These mutations led to the formation of *Es*AureoHA and *Es*AureoHS respectively.
256 Following primers were used to generate *Es*AureoHA and *Es*AureoHS constructs
257 respectively-
258 *Es*AureoHA_FP:5'CGCAACCGCGAAGCGGCGAAACGCAGC3', *Es*AureoHA_RP:5'GC

259 TGCGTTTCGCCGCTTCGCGGTTGCG3';*Es*AureoHS_FP:5'CGCAACCGCGAAAGCGC
260 GAAACGCAGC3' ; *Es*AureoHS_RP:5'GCTGCGTTTCGCGCTTTCGCGGTTGCG3'.

261 ***2.8 Overexpression and purification of WT and mutant proteins:*** *Es*Aureo1_wild and its
262 mutatants - *Es*AureoHA and *Es*AureoHS were transformed into the *Escherichia coli* C43
263 strain to express the wild type protein along with its mutants. Colonies obtained through
264 transformation were then inoculated into the kanamycin containing Luria-Bertani (LB)
265 (*HiMedia*) broth cultures and grown overnight at 37˚C. In each case, 1% inoculum was
266 transferred to the fresh media and grown at 37˚C till OD_{600} reached 0.6. Following IPTG
267 (*Promega*) induction, the cells were grown in the dark at 21˚C overnight. Bacterial cells were
268 then harvested by centrifugation at 8,000 rpm for 10 minutes. The cell pellet was then
269 dissolved in lysis buffer (20 mM Tris, pH 8; 10 mM NaCl; 10% Glycerol) and incubated with
270 protease inhibitor cocktail (*Sigma*), a pinch of lysozyme (*SRL*) and phenylmethylsulfonyl
271 fluoride (PMSF, *Promega*). The dissolved cell pellet was then subjected to ultrasonic
272 vibrations (*Hielscher*) and high-speed centrifugation (*Thermo Fisher Scientific*) at 12500 rpm
273 for 1 hour at 4˚C. Following centrifugation, the supernatant was collected and subjected to
274 Ni-NTA affinity chromatography (Qiagen). Following loading and wash, hexa-histidine
275 tagged protein fractions were eluted using the elution buffer (20 mM Tris, pH 8; 10 mM
276 NaCl; 100 mM Imidazole; 10% Glycerol). The eluted fractions containing the desired protein
277 were then subjected to PD-10 desalting column (*Sigma*) for the removal of excess imidazole.
278 The desalted protein was then concentrated using Amicon® Ultra Centrifugal Filter. The
279 quality of protein was checked using SDS-PAGE (*Bio-Rad*). Further purification by
280 Heparin/gel filtration chromatography resulted in extremely poor yield. Therefore, affinity
281 purified and desalted protein fractions were used for EMSA studies, carried out at least in
282 triplicates from multiple batches of protein purification. The concentration of the wild type as
283 well as the mutant proteins was specifically determined with respect to flavin [at 450 nm,
284 considering the extinction co-efficient of flavin (12500 $M^{-1}cm^{-1}$) using UV-Vis spectroscopy
285 (*Shimadzu*)].

286 ***2.9 Electrophoretic Mobility Shift Assay:*** HPLC purified and lyophilized single□stranded
287 oligonucleotides of 24bp containing 'Aureo-box' sequence, 'TGACGT', (FP:
288 5'TGTCCTTGGCTGACGTCAGCCAAGCAC3';RP:5'GTGCTTGGCTGACGTCAGCCA
289 AGGACA3') were purchased (*IDT*). Following resuspension in annealing buffer (10 mM
290 Tris, pH 8.0; 20 mM NaCl) the complementary DNA strands in equimolar amounts were
291 annealed by heating at 95˚C for 2 mins followed by gradual overnight cooling. The binding

292 buffer (50 mM Tris, pH 8.0; 50 mM NaCl; 1.25 mM $MgCl_2$; 0.01 mg/mL BSA; 20%
293 glycerol) was next added to the double stranded DNA (dsDNA) to achieve a final
294 concentration of 0.5 uM. Each protein was then serially diluted and added to the solution of
295 dsDNA and binding buffer mixture. A total of nine samples were prepared for protein-DNA
296 mixtures with varying protein concentrations. The substrate DNA minus protein was
297 considered as negative control. All samples including the control were incubated on ice under
298 BL for 45 minutes prior to the commencement of electrophoresis. The electrophoretic run
299 was performed using Bio-Rad's Mini-PROTEAN system at 4˚C under BL-illuminated
300 condition. The samples were resolved at 150 Volts at 4˚C for one hour. Upon the completion
301 of electrophoresis, the native gel was stained with SYBR Gold nucleic acid stain (*Thermo*
302 *Fisher Scientific*) for 45 minutes and imaged in the Bio-Rad ChemiDoc MP system.

303 **3. Results**

304 ***3.1. Sequence retrieval and analysis:***

305 A total number of 173 bZIP sequences inclusive of 78 from plants, 69 from opisthokonts and
306 26 from Aureos are considered [**SI-2**] herein to assess amino acid sequence
307 composition/conservation/variations. The conservation of leucines/non-polar amino acid
308 residues at every a/d position in the C-terminal dimerization domain/zipper region of Aureos
309 corroborate well with other bZIPs. However, we do observe few remarkable variations at the
310 N-terminal basic region of Aureo_bZIPs when compared with others. The basic region
311 responsible for DNA recognition possesses a signature sequence of nine amino acid residues
312 [N-$(X)_7$-K/R] [**SI-3**]. A histidine is uniquely found at the 4th position [N-$(X)_2$-**H**-$(X)_4$-R] of
313 the basic region in Aureos [**Figure-1.a**] unlike others. While in plant-bZIPs serine is the
314 invariable occupant (except plant bZIP subfamily D, F) [**SI-3.**]; alanine is mostly present in
315 opistokont bZIPs, excluding CREB, CREB3, ATF6 [**SI-3**]. Therefore, the basic region
316 sequence of opisthokont and plant bZIPs can be broadly designated as [N-$(X)_2$-**A**-$(X)_4$-K/R]
317 and [N-$(X)_2$-**S**-$(X)_4$-R] respectively. Notably in Aureo2, histidine is substituted with leucine
318 [**Figure-1.a**]. An in-depth investigation into all the Aureo further divulged that *Sj*Aureo2
319 despite being designated as a type-2 Aureo, possesses histidine [**SI-3**]. This observation can
320 be justified from the phyletic pattern [**Figure-1.b**], where *Sj*Aureo2 clubs with other Aureo
321 paralogs rather than the Aureo2 cluster. As neither histidine nor leucine is found at the
322 debatable 4th position in any other bZIP across three kingdoms of life, their persistence in
323 aureos could bear an evolutionary significance. Again, the presence of threonine as the 8th
324 residue in Aureo2 basic region [N-$(X)_2$-LA-$(X)_2$-**T**R] [**Figure-1.a**] is also notable considering

325 the presence of serine at the homologous position in most other Aureo bZIPs. Incidentally,
326 the 8th position of all bZIPs is occupied mostly by serine or cysteine. A covariation of
327 histidine at 4th and serine at the 8th position is further detected in the co-variation analysis
328 using GREMLIN (Kamisetty et al., 2013)[**Figure-1.c**]. This probably explains why both
329 histidine and serine are simultaneously replaced by leucine and threonine respectively in
330 Aureo-2 paralogs.

331 ***3.2 Phylogeny estimation and course of bZIP evolution*:**

332 The evolutionary position and the phylogenetic relationship of all selected 173 bZIP proteins
333 from plants, opisthokonts and Aureos can be inferred from the phylogenetic tree construction
334 [**Figure-2**]. However, the deeply rooted divergence within the ancient nodes may not have
335 been detected due to the comparatively shorter length of bZIP domains. Nevertheless, three
336 distinct lineages from a common ancestor have been observed. The first lineage includes
337 BATF, PAR, and E4BP4. The second lineage comprises opisthokont bZIP families such as
338 CREB2, ATF2, CEBP, ATF3, FRA, and FOS along with the viral bZIP family Zta. The
339 remaining plant and opisthokont bZIPs are found to cluster together with Aureo bZIPs in the
340 third lineage. However, the last common ancestor of the third lineage further diverges into
341 two distinct clades. One is solely represented by all Aureo_bZIPs, while the other splits
342 further into two branches: the opisthokont bZIPs (e.g., PAP, GCN4, JUN, MAF, CREB3,
343 CREB, and ATF6) and all plant bZIPs (e.g., A, B, C, D, E, F, G, H, I, and S). However, the
344 most appropriate sister clade or immediate ancestor of Aureo bZIPs could not be ascertained.
345 The phylogenetic tree of all bZIPs illustrates the tendency of Aureo_bZIPs to club together in
346 the same clade, forming a distinct sub-lineage without intermingling with bZIPs either from
347 plants or opisthokonts. Most Aureo paralogs within the Aureo-bZIP clade align by subtype,
348 with a few exceptions, while the remaining ones lose their distinctiveness and cluster
349 randomly [**Figure- 2**]. In summary, the phylogeny estimation of bZIPs from multiple
350 genomes not only identifies the ancestor-descendant relationships among different bZIP
351 members but also highlights the evolutionary relationship of Aureo_bZIPs with the rest.

352 **3.3. Network analysis and bZIP dimer stability towards substrate DNA interaction:**

353 Aureo bZIPs are unique in the sense that they are BL-regulated. In fact, the LOV → bZIP
354 signaling relies on an allosteric pathway (A. Banerjee, Herman, Serif, et al., 2016). The
355 resulting conformational changes at the bZIP-substrate DNA interface further promotes DNA
356 binding without much alteration in DNA binding affinity. In absence of full-length

experimental structure of any Aureo at dark and light states, it would be difficult to precisely identify the intervening residues that transduce light energy into DNA binding. Despite significant homology observed between bZIP and LOV domains individually with other bZIP/LOV members respectively, the existence of heterogeneous linkers with varying sequence composition and length further complicates this problem. While bZIP dimerization is an essential pre-requisite of DNA binding activity, Aureos contain the only bZIPs that are connected with a BL-sensor. Therefore, one crucial question is: how does an Aureo bZIP compare with other bZIPs? We therefore constructed all-atom networks from eight co-crystallized bZIP-DNA complexes. While centrality measures are frequently used for network analysis, in this study, we particularly focused on Eigenvector Centrality (EC) – especially given their implications in allostery (Negre et al., 2018). EC that considers both the number of connections made by a node as well as the flow of information associated with them, EC has been successfully used to identify residues responsible for allosteric communication in enzymes (Negre et al., 2018). We did not consider Aureo model structures for RIG analysis because structural artifacts could affect the result. We therefore calculated EC from networks constructed upon eight co-crystal structures of homo/heterodimeric bZIP-DNA complexes [PDB IDs: 1DH3, 1FOS, 1GD2, 1JNM, 1NWQ, 1YSA, 2H7H and 2WTY] [**SI-4**]. Residues with high EC values with Z(X) > 1.5 are only considered and marked in green [**Figure-3**]. Additionally, two to three residues from monomeric units showing highest EC values are color coded in red to check any further significance. The residues involved in DNA binding are marked in blue [**Figure-3**]. In all cases, residues with high EC values are found to congregate at the zipper region, albeit at variable distances from the basic region. Residues with highest EC values specifically occupy 'a' and 'd' positions of a heptad in every single case, as seen in the figure as well as multiple sequence alignment [**Figure-3.b**]. We find this result extremely interesting considering well-known hydrophobic interaction between residues at positions 'a' and 'd' towards leucine zipper dimerization, its stability as well as their contribution in allosteric regulation (Cruz et al., 2023). In terms of EC, after 'a' and 'd', the next important positions happen to be 'e' and 'g'. As emphasized in our earlier study (Khamaru et al., 2024), the electrostatic compatibility in between 'e' and 'g' can singularly govern bZIP homo/heteromerization(C. Vinson et al., 2002)(Krylov et al., 1994). Sequence comparison reveals that the homologous residues in Aureos corresponding to high EC values in other bZIPs are mostly conserved (similar if not identical) except for the 'd' position in the 4th heptad. This particular position in Aureo is occupied by polar or even charged amino acid residues, whereas this is always leucine in other bZIPs. Overall, our EC

391 analysis combined with sequence alignment reveals that Aureo zippers and the rest are
392 generally comparable. However, precise contribution of important heptad residues (a/d/e/g)
393 in allosteric regulations and/or signal transduction, as predicted by EC analysis, is subjected
394 to further experimental validations.

395 ***3.4. Decoding bZIP-DNA interactions - insights from modeled and docked Aureo subtypes*:**
396 Following *Es*Aureo1, *Es*Aureo2, *Es*Aureo3, *Es*Aureo4 and *Sj*Aureo5 homodimer modeling
397 and energy minimization, each one was subjected to *in silico* docking experiments with the
398 substrate DNA sequence encompassing a TGACGT core which is known to be the binding
399 sequence for Aureo bZIPs, termed as 'Aureo-box'. The best scoring complex structures were
400 selected and bZIP-DNA interfaces were characterized based on hydrogen bonding/salt
401 bridge/van der Waals' interactions, interface area and energy. The bZIP-DNA structures of
402 all five Aureo-bZIP representatives are depicted in [**Figure-4**]. The accuracy of our docked
403 structures was further assessed by checking their RMSD when superimposed with the
404 modeled/docked structure obtained through alpha fold. To test the reliability of our docked
405 structures, we conducted PDBePISA (Protein Interfaces, Surfaces and Assemblies) analysis
406 and compared them with experimental data on bZIP-DNA complex [1DH3 and 1FOS
407 representing homo- and heterodimer-DNA interactions respectively]. The emphasis was
408 given on three parameters – the interface area, solvation energy and number of non-covalent
409 interactions, precisely hydrogen bonding and salt bridge interactions. While the interface area
410 between monomeric units of protein chains ranges from ~900 $Å^2$-1200 $Å^2$ (homodimer to
411 heterodimer respectively), that between protein-DNA ranges from ~300-400 $Å^2$. A negative
412 value of gain in solvation free energy (Δ^iG) upon interface formation in both protein-
413 protein/DNA complex formations indicate positive affinity between them and the
414 hydrophobic interface. In the case of all homodimeric Aureos [*Es*Aureo1-4, *Sj*Aureo5], the
415 interface area is very similar to homodimeric 1DH3/1JNM, with an average of 915 $Å^2$.
416 Aureo-DNA interface area ranges in between ~350-450 $Å^2$ with a very similar number of
417 hydrogen bonding/salt bridge interactions like in experimental structures. Further, the Δ^iG for
418 both protein-protein/DNA in Aureo-DNA complexes are not only negative but the values are
419 very similar to those of native co-crystal structures. The N-terminal basic regions being the
420 key determinants behind DNA binding specificity of bZIPs, they were first screened for polar
421 including hydrogen bonding interactions with the DNA bases. At first a detailed analysis of
422 the hydrogen bonding interactions involving the basic region and the substrate DNA from
423 experimentally derived co-crystal structures of the bZIP-DNA complexes [**SI-5**] was

424 performed to determine the segment of bZIP crucial for the DNA binding and to identify the
425 crucial residues within the basic region that facilitate DNA binding. Analysis of the bZIP-
426 DNA interaction patterns of all the co-crystal structures revealed multifarious specificities of
427 bZIP proteins despite overall structure-sequence conservation. Since, the five subtypes of
428 Aureo_bZIPs exhibited minor difference in residue composition of the signature motif of
429 bZIP meant for DNA binding, all the five Aureo_bZIPs were docked with DNA [**Figure-4**]
430 and were then screened for the hydrogen bonds and polar interactions present between the
431 basic region residues and the substrate DNA bases to understand whether histidine takes part
432 in the interaction with DNA. In *Es*Aureo1-DNA complex, His362 (NE2) is found to interact
433 with dT'8. *Es*Aureo4 also exhibits interaction of His50 (NE2) with DNA. His153 (NE2) of
434 *Sj*Aureo5 interacts with OP2 of dG'6. All the polar interactions detected at the protein-DNA
435 interface of the docked structures are color coded and presented in tabular format [**SI-6**].

436 Characteristic of all bZIPs, in Aureo-DNA complexes too, the interactions between
437 asparagine and arginine/lysine and substrate DNA in the signature [N-$(X)_7$-K/R] sequence are
438 conserved. Additionally, interactions from basic amino acids towards substrate binding are
439 also prominent. Perhaps the most notable finding is the involvement of the histidine in DNA
440 binding activity in all cases. As already mentioned, the absence of histidine at the
441 homologous position of plant/opisthokont bZIPs led to further speculation about its possible
442 evolutionary impact on the origin and evolution of all Aureo in the bZIP superfamily.

443 **3.5 Exploring the importance of Histidine substitution by *in silico* mutageneis,**
444 **phylogeny and co-evolution analysis:**

445 To further understand the role of histidine at the N-terminal basic region of the Aureo bZIPs,
446 *in-silico* mutagenesis in sequence and structure was conducted. Histidine was mutated to
447 serine (as in plant bZIPs), alanine (as in opisthokont bZIPs) and leucine (as in Aureo2) to find
448 out the consequences in terms of evolution as well as DNA binding respectively. No
449 significant polar interaction or hydrogen bonding is found when His362 is mutated to alanine.
450 When leucine replaces His362/His153 in the docked *Es*Aureo1 / *Sj*Aureo5-DNA complex, no
451 interactions with any of the nucleotides can be seen. His51 in *Es*Aureo3, upon substitution by
452 leucine, remains in close contact with dG'6 of the substrate DNA. Similar situation arises in
453 *Es*Aureo4, where His50 upon mutation to leucine remains in close contact with dG'6.
454 However, no polar contacts could be observed in both these cases. His362 of *Es*Aureo1 on
455 being mutated to serine, comes in close contact with dC`7. While *Es*Aureo2's Leu197 to

456 serine mutation maintains dT'8 contact, His51→Ser in *Es*Aureo3, shows possible interaction
457 with the N7 of DG'6. Incorporation of serine at the homologous histidine positions in
458 *Es*Aureo4 and *Sj*Aureo5, fails to show any significant interaction. We must acknowledge that
459 the experimental 3D structure of the Aureo-DNA complex could be most reliable. However,
460 our modeled docked structures indicate an active role of His in Aureo-box DNA binding
461 activity. Single residue substitution can influence DNA binding affinity, as noticed in one of
462 our earlier collaborative studies – FD1/FD2 belonging to plant bZIP subfamily A, exhibited a
463 10-fold difference in DNA binding activity (Dutta et al., 2021). To elaborate further on single
464 histidine substitution, not only we performed MD simulations but also conducted *in vitro*
465 experiments with *Es*Aureo1_wild, *Es*Aureo1_HA and *Es*Aureo1_HS constructs – we discuss
466 the results in the subsequent section of this manuscript. We also wanted to check the
467 evolutionary significance of histidine at this specific position. Therefore, we re-constructed
468 the phylogenetic tree after altering the histidine/leucine position in Aureo by serine (similar
469 to plant bZIPs) and alanine (similar to opisthokont bZIPs). Very interestingly, upon serine
470 substitution, Aureos shift closer to the plant bZIPs sharing a common evolutionary lineage
471 with all the plant bZIP subgroups except D, F and H. All the opisthokont bZIPs are clustered
472 in a different lineage in this case [**Figure-5.a**]. Perhaps this is important to mention here that
473 plant bZIPs D, F and H differ from the remaining plant bZIPs at the crucial 4th/8th position
474 of basic region signature sequence. D and F plant bZIPs possess alanine instead of serine
475 [$N(X)_2\underline{A}(X)_5$], similar to opisthokont bZIPs [**SI-3**]. F and H bZIPs possess Y and A
476 respectively at the 8th position instead of typical serine [$N(X)_6\underline{Y/A}R$] [**SI-3**]. Upon mutation
477 to alanine, the bZIPs of Aureo aligned in a lineage with opisthokont and plant bZIPs, albeit
478 differently from the wild types. [**Figure-5.b**]. All through we considered a bootstrap value of
479 1000 to obtain statistically confident data. And indeed, the presence of histidine in Aureo
480 does make a difference in their evolutionary origin. Co-evolution studies conducted with
481 *Es*Aureo1 bZIP with an E-value cut-off 10^{-10} followed by Weblogo analysis shows distinct
482 presence of histidine [**Figure-1.c**] in Aureo subtypes. Upon increasing the E-value to 10^{-4} to
483 accommodate more bZIP sequences however led to complete disappearance of histidine and
484 appearance of serine/alanine at the homologous position [**Figure-5.c**].

485 ***3.6 Probing the Dynamics of bZIP-DNA Interactions through Molecular Dynamics (MD)***
486 ***Simulations:***

487 MD simulations were performed to understand the consistency of interaction between
488 *Es*Aureo1_wild, *Es*Aureo1_HA and *Es*Aureo1_HS and the substrate DNA, albeit over a short

489 time scale. We particularly monitored the behaviour of residue 362 (His, Ala and Ser
490 respectively) throughout the MD run. Thus, the post-simulation analyses conducted include
491 RMSD (Root Mean Square Deviation), RMSF (Root Mean Square Fluctuation), the radius of
492 gyration (Rg), Number of Contacts (within 3 nm cutoff) and the number of hydrogen bonds.

493 **3.6.1. RMSD**

494 The RMSD of the protein backbone (Cα-atoms) was analyzed from the simulation data and
495 plotted to compare structural stability across variants. Notably, *Es*Aureo1_wild exhibited
496 consistently lower deviation compared to the mutant variants (*Es*Aureo1_HA and
497 *Es*Aureo1_HS), with average RMSD values of 0.346 nm, 0.395 nm, and 0.414 nm,
498 respectively [**Figure-6.a**]. While all variants showed similar deviation trends at the outset, the
499 wild type demonstrated a marked decrease in deviation around 5 ns, contrasting with the
500 rising trends observed in the mutants. A transient surge in deviation for *Es*Aureo1_wild
501 occurred near 17 ns, followed by alignment with mutant trends between 25 and 30 ns. After a
502 minor fluctuation around 30 ns, the wild type resumed its low-deviation profile, maintaining
503 this trend until the end of the simulation (60 ns). Notably, the *Es*Aureo1_HS variant exhibited
504 a significant increase in RMSD between 50 and 60 ns, stabilizing at a higher deviation. These
505 observations underscore the structural resilience of *Es*Aureo1_wild compared to its mutants.

506 **3.6.2 RMSF**

507 To determine the flexibility of the protein residues, especially His362, the RMSF data was
508 elucidated and plotted against the simulation runtime. A subtle variation, commonly
509 suspected to arise from differences in binding dynamics and solvent interactions, is generally
510 expected between protein chains C and D of the homodimer; hence, they were analyzed and
511 plotted separately [**Figure-6.c,d**]. In both polypeptide chains of Aureo-dimer, His362 of
512 *Es*Aureo1_wild shows the least flexibility, followed by Ala362 of *Es*Aureo1_HA and then
513 Ser362 of *Es*Aureo1_HS.

514 **3.6.3 Radius of gyration**

515 The Rg represents the overall compactness of the protein by measuring the average distance
516 of its atoms from an imaginary axis passing through its center of gravity. Analysis of the Rg
517 curves [**Figure-6.b**] reveals that *Es*Aureo1_wild exhibits greater compactness throughout the
518 simulation compared to its mutant counterparts. Up to the 30 ns mark, all variants display a
519 similar trend, but beyond this point, the wild-type variant maintains a consistency of its Rg,
520 indicating a more compact structure with minimal fluctuation. In contrast, the *Es*Aureo1_HA
521 and *Es*Aureo1_HS mutants show increased fluctuations and less compact conformations over
522 time. Notably, the *Es*Aureo1_HS variant exhibits a sudden and significant drop in Rg after

523 the 50 ns mark, reflecting a collapse in compactness that correlates with the sharp rise in
524 RMSD observed in the same time frame. This behavior underscores the distinct dynamic
525 stability of the wild variant compared to its mutants till the end of the simulation (60 ns).

526 **3.6.4. State of hydrogen bonds**

527 The variation in the number of hydrogen bonds made by His362 with the DNA in both the
528 wild and mutant variants was obtained and was plotted against the simulation time (60000ps).
529 According to the graphs, the residue His362 of *Es*Aureo1_wild shows the maximum number
530 of hydrogen bonds, fluctuating between 0 to 4 [**Figure-7.a**]. The residue Ser362 of
531 *Es*Aureo1_HS shows a moderate number of H-bonds throughout the simulation, fluctuating
532 between 0 to 3 [**Figure-7.b**]. The residue Ala362 of EsAureo1_HA shows no H-bonds
533 throughout the simulation period with the DNA [**Figure-7.c**]. Hydrogen bonding interactions
534 were visualized from the post-MD trajectory files, using PyMOL, with a 10ns interval
535 between each state analyzed for an overall period of 60ns [**Figure-8**].

536

537 ***3.7. In vitro protein-DNA interaction study by Electrophoretic Mobility Shift Assay:***

538 EMSA was performed with the purified and desalted samples of *Es*Aureo1_wild along with
539 its two mutants - *Es*Aureo_HS and *Es*Aureo_HA to compare their DNA binding ability under
540 BL. In all cases, the shift from unbound to substrate DNA bound state was observed with the
541 increase in concentrations of protein [**Figure-9**]. Presence of free DNA bands are indicative
542 of protein being unbound with its substrate DNA. Gradual disappearance of free DNA bands
543 and the resultant shift in electrophoretic mobility is indicative of protein-DNA complex
544 formation. The highest concentration of *Es*Aureo1_wild at which an unbound DNA band was
545 evident first was 0.04 μM [**Figure-9.a**]. In the case of *Es*Aureo_HS [**Figure-9.b**] and
546 *Es*Aureo_HA [**Figure-9.c**], the first presence of an unbound DNA band showed up at
547 concentrations 0.076 μM and 0.082 μM respectively. Hence, although all of the variants
548 manifest DNA binding, the result of EMSA indicates that *Es*Aureo1_wild has a higher DNA
549 binding affinity. And the unique presence of histidine at the basic region of Aureo bZIPs
550 seems justifiable for their specific interaction with Aureo-box substrates.

551 **4. Discussion**

552 The global network of TFs comprising interactions with specific substrate DNA or partner
553 protein molecules regulates one of the most fundamental processes of life - gene expression.
554 Besides the possibility of simple/auto-regulation, a TF can participate in feed forward

555 loops/feedback loops (FFLs/FBLs)(Alon, 2007) as homodimer or heterodimer, in complex
556 and dynamic gene expression regulatory units [**Figure-10**]. While the orderliness and
557 sequence composition of the basic and fork regions of bZIPs play a crucial role in DNA
558 binding specificity, sequence organization and stability of heptad repeats in the zipper region
559 is equally important. Even a subtle change in heptad sequence can impact dimerization
560 specificity and stability, and the resulting manifestation could be significant. Choosing
561 partners from the same or different group of bZIPs, respectively for homo- and hetero-
562 dimerization can generate substantial functional diversity. The 3D structure of a protein can
563 be considered as a network of nodes (amino acid residues) connected via edges (non-covalent
564 interactions) and the relative importance of the individual amino acid residues can be
565 obtained by calculating different topological parameters of RIG. Therefore, apart from
566 characterizing protein-protein/DNA interface in terms of bonding interactions, surface area
567 and energy, we conducted all-atom network analysis. Centrality measures like degree,
568 closeness and betweenness effectively captures influential nodes in a network. In this study,
569 we emphasized on measuring EC values considering its potential to detect nodes important
570 for making connections and information flow, especially allostery. Interestingly, residues
571 with highest EC values are always at 'a' and 'd' positions of a heptad in all eight
572 representative co-crystal structures. Importance of hydrophobic residues at the strategic
573 positions necessary for dimerization and consequent enhancement of DNA binding activity
574 has been shown for c-Fos mutants(Porte et al., 1997). Incorporation of isoleucine at the 2nd
575 heptad not only promoted homodimerization but also conferred DNA binding specificity
576 towards TRE substrate in c-Fos mutants. While EC calculations for Aureos await
577 determination of experimental 3D structures, sequence comparison does indicate that Aureo
578 bZIPs are mostly similar to other bZIPs at least in these specific nodes except 'd' residue in
579 heptad 4. Measurement of EC undoubtedly reiterates the importance of hydrophobic residues
580 towards maintaining stable bZIP dimerization, signal transfer and thereby promoting DNA
581 binding activity. Therefore, insights obtained from EC measurements could be helpful for
582 designing synthetic sensory TF in the near future.

583 The BL-responsive sensory TFs like Aureo, the pivot of this study, comes with an additional
584 advantage. Such an association of one major group of eukaryotic TF (here, bZIPs) with a
585 light sensor (here, LOV) is rare and fascinating. Our study therefore attempts to draw a
586 comparative analysis of Aureos and the other conventional bZIP proteins without LOV
587 sensors. With distinct differences noticed, it remains to be clarified whether or not these

588 variations arose through evolutionary acquisition of the sensor domain to confer
589 physiological advantages to the host organisms. Though bZIPs are supposed to have far
590 reaching origin, the expansion and diversification of the bZIP superfamily has been found to
591 be positively correlated with the evolution of eukaryotes (Jindrich & Degnan, 2016). The
592 number of bZIP homologs as well as the complexity of bZIPs have increased over the time in
593 the process of evolution. Initially bZIPs were supposed to evolve independently in 4
594 eukaryotic lineages – planta, opisthokonta, amoebozoa, and heterokonta (Jindrich & Degnan,
595 2016). Among them 17 bZIP subfamilies within opisthokont, namely, YAP, MAF, XBP1,
596 CNC, BATF, CREB, CREB-2, OASIS, PAR, E4BP4, ATF-2, ATF-4, ATF-6, FOS, JUN,
597 C/EBP, PAP (Amoutzias et al., 2007) (Fujii et al., 2000) and ten distinct subclasses (A, C, D,
598 G and S) of plant bZIPs (Jakoby et al., 2002) (Corrêa et al., 2008) are evident. Whereas in
599 heterokontophyta (**SI-7]**, the phylum comprising of 12 families under the algal group-4
600 as proposed in the algal classification by Robert Lee (Lee, 2018), the most abundant bZIP
601 transcription factor is Aureo (Rayko et al., 2010). It has been observed in the evolutionary
602 analysis performed by us that all the bZIPs of different Aureo homologs together form a
603 different clade albeit shared the ancestor with opishtokont bZIP subfamilies- JUN, MAF,
604 CREB, CREB3, PAP, GCN4 and plant bZIP subfamilies. But substitution of histidine results
605 in an assembly of Aureo-bZIPs predominantly with plant bZIPs sharing a common ancestral
606 lineage. This study therefore investigates how nuances at the residue level are manifested in
607 the phyletic distribution of bZIP members, including the evolution of Aureos and their
608 subtypes.

609 The bZIPs of the metazoans recognize 6 different consensus DNA-binding sites- c-AMP
610 responsive element (CRE- TGACGTCA), TPA responsive element (TRE- ATGAGTCAT),
611 CAAT box (TTGCGCAA), PAR binding sites (TTACGTAAT), Maf recognition element
612 (MARE- CTGATCAGC) and CRE-like elements (TGACGTGC) (Amoutzias et al., 2007)
613 (Rodríguez-Martínez et al., 2017). Again, CRE, TRE and YAP (yeast activator protein) sites
614 can be recognized by fungal bZIPs. Plant bZIPs recognize G-box (CACGTG), A-box
615 (TACGTA), C-box (GACGTC), S-box (TGACGTG), D-box (TGACGTG) (Wang et al.,
616 2018) etc. We conducted *in-silico* and *in-vitro* studies, using Aureo-box containing CRE
617 (TGACGTCA) as the substrate DNA [sequence taken from X-ray structure of CREB bZIP-
618 CRE complex, PDB ID: 1DH3]. The docking, MD simulation as well as EMSA studies were
619 performed not only to check the DNA binding efficiency of the Aureo_bZIPs (wild type and
620 mutants) but also to explore the precise role of histidine in DNA binding. Both theory and

621 experiments indicate significance of histidine at the basic region of aureochrome. It can be
622 concluded that His362 plays a key role in positioning the *Es*Aureo1 bZIP to the core ACGT
623 sequence by favorably interacting with its flanking sequence. Changing this amino acid to
624 Ser (as in plants) and Ala (as in opisthokonts) leads to a significant decrease in polar
625 interactions [**Figure-7,8**] [**SI-8**] and therefore impacts the stability of the complex [**Figure-**
626 **6.a**] [as found from MD Simulation study]. However, at the same time, the overall binding
627 strength of all the constructs remains comparable [as confirmed by the EMSA studies]
628 [**Figure-9**]. This makes it clearer that His is very strongly related to the Aureo box, and thus
629 the slightest change in this recognition box (as seen in opisthokonts and plants) makes this
630 amino acid residue site prone to change. This provides an answer for the causality of co-
631 evolution. It is worth reiterating that Aureos are light-responsive TFs and therefore should
632 function like a photo-switch. Studies regarding the kinetics of binding and the width of
633 spectrum of the changes in functionality of the bZIP due to variation in substrate DNA
634 sequence, are still an area requiring further work. The binding specificity of a TF to DNA is
635 intricately governed by its interaction with the minor groove geometry and regional
636 electrostatics. Among the three mutants analyzed through simulation, *Es*Aureo1_wild has the
637 maximum DNA binding ability with the highest number of hydrogen bonds present at the
638 bZIP-DNA interface. *Es*Aureo1_HS ranks in between wild type and *Es*Aureo1_HA. The
639 alanine mutant modeled after opisthokont bZIP proteins, emerged as distinct, with Ala362
640 failing to interact with the flanking residues of the ACGT core. While the number of non-
641 covalent interactions, e.g. hydrogen bonds, determines DNA binding specificity(Lin & Guo,
642 2019), prompt and selective binding is eventually reflected in protein-DNA association
643 kinetics. Molecular docking, MD simulation as well as EMSA studies reveal that the
644 placement of histidine bespoke 'Aureo-box' specific interaction. However, it would be highly
645 interesting to see whether histidine makes any difference in association kinetics of Aureos
646 towards substrate recognition/binding upon BL illumination. Strength and specificity of DNA
647 binding interactions as well as variable association kinetics can be adopted further for
648 developing precision optogenetic tools.

649 Perhaps another important observation that we made in this study is the unique presence of
650 histidine in all Aureo bZIPs, except Aureo2 from several stramenopiles. Moreover, Aureo2
651 also possesses non-functional LOV (Takahashi et al., 2007). Out of eleven conserved amino
652 acids in the flavin-binding pocket, nine are conserved in Aureo2. The reason behind such
653 differences in Aureo2 is elusive – it is possible that the sensor domain of Aureo2 could be an

654 intermediate between non-light sensing PAS (Per-ARNT-Sim, ancestor to LOV) and LOV.
655 Our study further unveiled that histidine co-evolves with serine at the 8th position of the
656 signature bZIP sequence. Interestingly in Aureo2, both 4th and 8th positions are differently
657 occupied by leucine and threonine respectively. Despite such marked changes in the basic
658 region, Aureo2 clubs with the rest Aureos in the phylogenetic tree and not with
659 plants/opisthokonts. However, upon single substitution from leucine to alanine, Aureo2 shifts
660 lineage and sides with CEBPs of opisthokonts, while retaining proximity with other Aureos.
661 Considering the presence of non-functional sensor domain and close association with
662 opisthokont bZIPs just upon single amino acid substitution, we speculate that Aureo2 might
663 have evolved first among the Aureos. During the course of evolution, possibly with the gain
664 of function mutation, Aureos have finally acquired the ability to sense light and perform light
665 dependent transcriptional activities. And perhaps to preserve this very important property,
666 several other Aureo paralogs emerged through gene duplication events.

667 In summary, the bZIPs of aureochromes share close structural and functional similarities with
668 other bZIP TFs found across plants and animals, exhibiting comparable dimerization
669 properties and DNA-binding affinities to substrate DNA. Consequently, this bZIP integrated
670 with its blue light sensor, can be utilized in plants and animals either as a genetically encoded
671 recombinant protein driven by a synthetic promoter or as a transgene expressed under native
672 promoters in target cells to achieve tissue-specific gene regulation via light stimulation.
673 Furthermore, orthogonal manipulation through engineered gene regulatory circuits can
674 facilitate non-invasive control over existing regulatory networks. Our previous study
675 indicates that the aureochrome-bZIP monomer dimerizes with bZIP monomers within the
676 aureochrome family as well as with other non-aureochrome bZIPs (Khamaru et al., 2024). As
677 such, introducing light-sensitive aureochrome-bZIPs into genetically modified transgenic
678 lines or transiently transformed cells, can enable light-mediated regulation of developmental
679 pathways and stress responses by interacting with the inherent bZIP proteins of plants or
680 animals. Additionally, all the bZIP proteins regulate crucial developmental processes of
681 plants and animals like- growth, cell division, and differentiation can be further modulated by
682 adjusting the duration of gene activation or repression through fine tuning of the light sensor
683 module associated with these bZIPs. Interestingly, all the subclasses of plant bZIP proteins
684 that bind to promoter or regulator present upstream of the target genes, recognize the ACGT
685 sequence of DNA. As Aureo-bZIPs also recognizes ACGT sequences, it seems to be a
686 promising optogenetic tool for regulating plant gene expression and influencing the existing

687 bZIP dependent metabolic and developmental pathways within plant kingdom. Thus,
688 characterization of these exclusive light regulated bZIPs not only gives insight to the
689 transcriptional regulation pattern of the lower group of plants i.e. the heterokont algae, but
690 shed light into the scope of optogenetic regulation of plant genes.

691 **Figure Legends**

692 **Figure-1**:

693 a. Multiple sequence alignment of the bZIP domains of Aureos
694 b. Phylogenetic tree comprising all the aureochrome homologs.
695 c. Weblogo result of the co-evolution study of aureochrome1 at E-value cut-off 10^{-10}.
696

697 **Figure-2**:

698 Phylogenetic tree of the bZIPs from plants, opisthokonts and Aureos. Different
699 subgroups of bZIPs are represented by different colours. Highest to lowest bootstrap
700 values are colour coded as green and red respectively.

701 **Figure-3**:

702 a. DNA-bZIP complex where the residues identified as important from eigenvector
703 centrality measure are colour coded. Green colour denotes EC value higher than 1.5,
704 Red colour indicates knob like structure (d & a) with the highest EC value, blue
705 colour represents DNA binding residues.
706 b. Multiple sequence alignment showing DNA binding residues (coloured blue) and
707 residues with higher EC values (coloured green/red).

708 **Figure-4:**

709 Docked bZIP structures of *Ectocarpus siliculosus* (*Es*) aureochrome1 (gray),
710 aureochrome2 (pale green), aureochrome3 (yellow), aureochrome4 (pink) and
711 *Saccharina japonica* (*Sj*) aureochrome5 (teal) bZIPs in complex with substrate DNA
712 sequences containing 'Aureo-box', TGACGT motif. Interactions between amino acid
713 residues of the DNA recognizing the basic region of bZIPs and the corresponding
714 nucleotide of substrate DNA are labeled.

715 **Figure-5**:

716 a. Re-construction of phylogenetic tree upon mutation of Aureos' histidine to serine
717 (plant like)
718 b. Re-construction of phylogenetic tree upon mutation of Aureos' histidine to alanine
719 (opisthokont like)
720 c. Weblogo result obtained from co-evolution study at E-value cut-off $10^{-4.}$
721

722 **Figure 6**:

723 a. Root Mean Square Deviation (RMSD) in nm plotted for *Es*Aureo1_wild (green),
724 *Es*Aureo1_HS (blue) and *Es*Aureo1_HA (orange) protein backbone for 60 ns
725 timescale of MD simulation.
726 b. Radius of Gyration (Rg) in nm for *Es*Aureo1_wild (green), *Es*Aureo1_HS (blue) and
727 *Es*Aureo1_HA (green) plotted against the simulation time of 60 ns.
728 c. Root Mean Square Fluctuation (RMSF) of the protein residues for *Es*Aureo1_wild
729 (orange), *Es*Aureo1_HS (green) and *Es*Aureo1_HA (yellow), as obtained from 60ns
730 simulation data, for Protein chain C.
731 d. Root Mean Square Fluctuation (RMSF) of the protein residues for *Es*Aureo1_wild
732 (orange), *Es*Aureo1_HS (green) and *Es*Aureo1_HA (yellow) for Protein Chain D as
733 obtained from 60 ns simulation data.
734 *[EsAu1 has been used as the abbreviation of EsAureo1]

735 **Figure 7**:

736 a. Average number of intermolecular hydrogen bonds between His362 in
737 *Es*Aureo1_wild and DNA during 60 ns timescale.
738 b. Average number of intermolecular hydrogen bonds between Ser362 in *Es*Aureo1_HS
739 and DNA
740 c. Average number of intermolecular hydrogen bonds between Ala362 in *Es*Aureo1_HA
741 and DNA.
742 *[EsAu1 has been used as the abbreviation of EsAureo1]

743 **Figure 8**:

744 Post-simulation visualization of Residue 362 and its hydrogen bonding interaction
745 with DNA (shown in yellow dashed line), at timesteps of 10, 20, 30, 40, 50 and 60ns

(from left to right). a. *Es*Aureo1_wild in green, b. *Es*Aureo1_HS in blue, c. *Es*Aureo1_HA in orange. *[*Es*Au1 has been used as the abbreviation of *Es*Aureo1]

Figure 9:

In vitro protein□DNA interaction study of Aureochrome_bZIPs through electrophoretic mobility shift assay-a. *Es*Aureo1_wild, b. *Es*Aureo_HS, c. *Es*Aureo_HA.

Figure 10:

Cartoon and diagrammatic representation of the sensory transcription regulation network, where Aureochrome is perceived to act as a sensory, blue-light regulated transcription factor regulating gene expression. The concept of sensory transcription regulation network is adopted from Network motifs: theory and experimental approaches by Alon U. [ref. 56, doi:10.1038/nrg2102]

Acknowledgement

MK and AD acknowledge University Grants Commission (UGC) and Department of Biotechnology (DBT), Government of India respectively, for their doctoral research fellowships. DM acknowledges funding from DBT, Government of India (BT/PR26435/BRB/10/1627/2017) for supporting the research work during the initial phase and SERB, Govt of India (CRG/2023/006463) at the present phase. The authors acknowledge the central instrumentation facility as well as the computer facility of the department supported by DBT-BUILDER and DST-FIST programs respectively. The authors also thank Soumen Roy, Bose Institute - Kolkata for important discussions on network analysis.

Declaration of interests

The authors declare no conflict of interest. No competing interest.

Author contribution

Madhurima Khamaru: Data curation, Investigation, Methodology, Formal analysis, Validation, Visualization, Writing – original draft, Writing – review and editing; **Debarshi Bose**: Investigation, Methodology, Formal analysis, Visualization, Writing – original draft; **Anwesha Deb**: Investigation, Methodology; **Devrani Mitra**: Conceptualization, Supervision, Funding acquisition, Project administration, Investigation, Methodology, Formal analysis, Validation, Visualization, Writing – original draft, Writing – review and editing.

Data availability statement:

All data generated or analyzed during this study are included in the main text article as well as in the supplementary information. Further enquiries can be directed to the corresponding author.

References

Alon, U. (2007). Network motifs: theory and experimental approaches. *Nature Reviews Genetics 2007 8:6*, *8*(6), 450–461. https://doi.org/10.1038/nrg2102

Altschul, S. F., Gish, W., Miller, W., Myers, E. W., & Lipman, D. J. (1990). Basic local alignment search tool. *Journal of Molecular Biology*, *215*(3), 403–410. https://doi.org/10.1016/S0022-2836(05)80360-2

Amoutzias, G. D., Veron, A. S., Weiner, J., Robinson-Rechavi, M., Bornberg-Bauer, E., Oliver, S. G., & Robertson, D. L. (2007). One billion years of bZIP transcription factor evolution: Conservation and change in dimerization and DNA-binding site specificity. *Molecular Biology and Evolution*, *24*(3), 827–835. https://doi.org/10.1093/molbev/msl211

Apweiler, R., Bairoch, A., Wu, C. H., Barker, W. C., Boeckmann, B., Ferro, S., Gasteiger, E., Huang, H., Lopez, R., Magrane, M., Martin, M. J., Natale, D. A., O'Donovan, C., Redaschi, N., & Yeh, L. S. L. (2018). UniProt: the universal protein knowledgebase. *Nucleic Acids Research*, *46*(5), 2699–2699. https://doi.org/10.1093/NAR/GKY092

Bader, A. G., & Vogt, P. K. (2006). Leucine Zipper Transcription Factors: bZIP Proteins. In *Encyclopedic Reference of Genomics and Proteomics in Molecular Medicine* (pp. 964–967). Springer Berlin Heidelberg. https://doi.org/10.1007/3-540-29623-9_2180

Banerjee, A., Herman, E., Kottke, T., & Essen, L. O. (2016). Structure of a Native-like Aureochrome 1a LOV Domain Dimer from Phaeodactylum tricornutum. *Structure*, *24*(1), 171–178. https://doi.org/10.1016/j.str.2015.10.022

Banerjee, A., Herman, E., Serif, M., Maestre-Reyna, M., Hepp, S., Pokorny, R., Kroth, P. G., Essen, L.-O., & Kottke, T. (2016). Allosteric communication between DNA-binding and light-responsive domains of diatom class I aureochromes. *Nucleic Acids Research*, *44*(12), 5957–5970. https://doi.org/10.1093/nar/gkw420

Banerjee, S., & Mitra, D. (2020). Structural Basis of Design and Engineering for Advanced Plant Optogenetics. *Trends in Plant Science*, *25*(1), 35–65. https://doi.org/10.1016/j.tplants.2019.10.002

Boral, A., Khamaru, M., & Mitra, D. (2022). Designing synthetic transcription factors: A structural perspective. *Advances in Protein Chemistry and Structural Biology*, *130*. https://doi.org/10.1016/BS.APCSB.2021.12.003

Busch, S. J., & Sassone-Corsi, P. (1990). Dimers, leucine zippers and DNA-binding domains. *Trends in Genetics*. https://doi.org/10.1016/0168-9525(90)90071-D

Cock, P. J. A., Antao, T., Chang, J. T., Chapman, B. A., Cox, C. J., Dalke, A., Friedberg, I., Hamelryck, T., Kauff, F., Wilczynski, B., & De Hoon, M. J. L. (2009). Biopython: freely available Python tools for computational molecular biology and bioinformatics. *Bioinformatics (Oxford, England)*, *25*(11), 1422–1423. https://doi.org/10.1093/BIOINFORMATICS/BTP163

Corrêa, L. G. G., Riaño-Pachón, D. M., Schrago, C. G., Vicentini dos Santos, R., Mueller-Roeber, B., & Vincentz, M. (2008). The Role of bZIP Transcription Factors in Green Plant Evolution: Adaptive Features Emerging from Four Founder Genes. *PLoS ONE*, *3*(8), e2944. https://doi.org/10.1371/journal.pone.0002944

Costa, B., Sachse, M., Jungandreas, A., Bartulos, C. R., & Gruber, A. (2013). Aureochrome 1a Is Involved in the Photoacclimation of the Diatom Phaeodactylum tricornutum. *PLoS ONE*, *8*(9). https://doi.org/10.1371/journal.pone.0074451

Cruz, P., Paredes, N., Asela, I., Kolimi, N., Molina, J. A., Ramírez-Sarmiento, C. A., Goutam, R., Huang, G., Medina, E., & Sanabria, H. (2023). Domain tethering impacts dimerization and DNA-mediated allostery in the human transcription factor FoxP1. *The Journal of Chemical Physics*, *158*(19). https://doi.org/10.1063/5.0138782

Deb, A., Grewal, R. K., Roy, S., & Mitra, D. (2020). Residue interaction dynamics in Vaucheria aureochrome1 light-oxygen-voltage: Bridging theory and experiments. *Proteins*, *88*(12), 1660–1674. https://doi.org/10.1002/PROT.25984

Delano, W. (2002). *The PyMOL Molecular Graphics System*.

Deppmann, C. D., Acharya, A., Rishi, V., Wobbes, B., Smeekens, S., Taparowsky, E. J., & Vinson, C. (2004). Dimerization specificity of all 67 B-ZIP motifs in Arabidopsis thaliana : a comparison to Homo sapiens B-ZIP motifs. *Nucleic Acids Research*, *32*(11), 3435–3445. https://doi.org/10.1093/NAR/GKH653

Duan, L., Hope, J. M., Guo, S., Ong, Q., François, A., Kaplan, L., Scherrer, G., & Cui, B. (2018). Optical Activation of TrkA Signaling. *ACS Synthetic Biology*, *7*(7), 1685–1693. https://doi.org/10.1021/ACSSYNBIO.8B00126/SUPPL_FILE/SB8B00126_SI_001.PDF

Dutta, S., Deb, A., Biswas, P., Chakraborty, S., Guha, S., Mitra, D., Geist, B., Schäffner, A. R., & Das, M. (2021). Identification and functional characterization of two bamboo FD gene homologs having contrasting effects on shoot growth and flowering. *Scientific Reports*, *11*(1). https://doi.org/10.1038/S41598-021-87491-6

Evgeny, K. (2010). Crystal contacts as nature's docking solutions. *Journal of Computational Chemistry*, *31*(1), 133–143. https://doi.org/10.1002/JCC.21303

Fujii, Y., Shimizu, T., Toda, T., Yanagida, M., & Hakoshima, T. (2000). *letters Structural basis for the diversity of DNA recognition by bZIP transcription factors*.

Glover, J. N. M., & Harrison, S. C. (1995). Crystal structure of the heterodimeric bZIP transcription factor c-Fos–c-Jun bound to DNA. In *Nature*. https://doi.org/10.1038/373257a0

Grigoryan, G., & Keating, A. E. (2006). Structure-based Prediction of bZIP Partnering Specificity. *Journal of Molecular Biology*, *355*(5), 1125–1142. https://doi.org/10.1016/j.jmb.2005.11.036

Hagberg, A. A., Schult, D. A., & Swart, P. J. (2008). Exploring network structure, dynamics, and function using NetworkX. *7th Python in Science Conference (SciPy 2008)*, 11–15. https://www.bibsonomy.org/bibtex/272096c6553d7057409fe78ca698eb332/mschuber

Hakoshima, T. (2005a). Leucine Zippers. In *Encyclopedia of Life Sciences*. John Wiley & Sons, Ltd. https://doi.org/10.1038/npg.els.0005049

Hakoshima, T. (2005b). Leucine Zippers. In *Encyclopedia of Life Sciences*. https://doi.org/10.1038/npg.els.0005049

Harbury, P. B., Zhang, T., Kim, P. S., & Alber, T. (1993). A switch between two-, three-, and four-stranded coiled coils in GCN4 leucine zipper mutants. *Science (New York, N.Y.)*, *262*(5138),

1401–1407. https://doi.org/10.1126/SCIENCE.8248779

Heintz, U., & Schlichting, I. (2016). Blue light-induced LOV domain dimerization enhances the affinity of aureochrome 1a for its target DNA sequence. *ELife*, *5*(JANUARY2016). https://doi.org/10.7554/ELIFE.11860

Hepp, S., Trauth, J., Hasenj, S., Bezold, F., Essen, L.-O., & Taxis, C. (2020). *An Optogenetic Tool for Induced Protein Stabilization Based on the Phaeodactylum tricornutum Aureochrome 1a LighteOxygeneVoltage Domain*. https://doi.org/10.1016/j.jmb.2020.02.019

Hepp, S., Trauth, J., Hasenjäger, S., Bezold, F., Essen, L. O., & Taxis, C. (2020). An Optogenetic Tool for Induced Protein Stabilization Based on the Phaeodactylum tricornutum Aureochrome 1a Light–Oxygen–Voltage Domain. *Journal of Molecular Biology*. https://doi.org/10.1016/j.jmb.2020.02.019

Huang, Y., Wang, L., Zheng, M., Zheng, L., Tong, Y., & Li, Y. (2014). Overexpression of NgAUREO1, the gene coding for aurechrome 1 from Nannochloropsis gaditana, into Saccharomyces cerevisiae leads to a 1.6-fold increase in lipid accumulation. *Biotechnology Letters*, *36*(3), 575–579. https://doi.org/10.1007/s10529-013-1386-0

Huysman, M. J. J., Fortunato, A. E., Matthijs, M., Costa, B. S., Vanderhaeghen, R., Van den Daele, H., Sachse, M., Inzé, D., Bowler, C., Kroth, P. G., Wilhelm, C., Falciatore, A., Vyverman, W., & De Veylder, L. (2013). AUREOCHROME1a-Mediated Induction of the Diatom-Specific Cyclin dsCYC2 Controls the Onset of Cell Division in Diatoms (Phaeodactylum tricornutum). *The Plant Cell*, *25*(1), 215–228. https://doi.org/10.1105/tpc.112.106377

Jakoby, M., Weisshaar, B., Dröge-Laser, W., Vicente-Carbajosa, J., Tiedemann, J., Kroj, T., & Parcy, F. (2002). bZIP transcription factors in Arabidopsis. *Trends in Plant Science*, *7*(3), 106–111. https://doi.org/10.1016/S1360-1385(01)02223-3

Jerng, H. H., Patel, J. M., Khan, T. A., Arenkiel, B. R., & Pfaffinger, P. J. (2021). Light-regulated voltage-gated potassium channels for acute interrogation of channel function in neurons and behavior. *PLOS ONE*, *16*(3), e0248688. https://doi.org/10.1371/JOURNAL.PONE.0248688

Ji, C., Mao, X., Hao, J., Wang, X., Xue, J., Cui, H., & Li, R. (2018). Analysis of bZIP transcription factor family and their expressions under salt stress in Chlamydomonas reinhardtii. *International Journal of Molecular Sciences*, *19*(9). https://doi.org/10.3390/ijms19092800

Jindrich, K., & Degnan, B. M. (2016). The diversification of the basic leucine zipper family in eukaryotes correlates with the evolution of multicellularity Genome evolution and evolutionary systems biology. *BMC Evolutionary Biology*, *16*(1), 1–12. https://doi.org/10.1186/s12862-016-0598-z

Kamisetty, H., Ovchinnikov, S., & Baker, D. (2013). Assessing the utility of coevolution-based residue-residue contact predictions in a sequence- and structure-rich era. *Proceedings of the National Academy of Sciences of the United States of America*, *110*(39), 15674–15679. https://doi.org/10.1073/PNAS.1314045110/SUPPL_FILE/SD05.XLSX

Khamaru, M., Nath, D., Mitra, D., & Roy, S. (2024). Assessing Combinatorial Diversity of Aureochrome Basic Leucine Zippers through Genome-Wide Screening. *Cells, Tissues, Organs*, *213*(2), 133–146. https://doi.org/10.1159/000527593

Kroth, P. G., Wilhelm, C., & Kottke, T. (2017). An update on aureochromes_ Phylogeny – mechanism – function. *Journal of Plant Physiology*, *217*, 20–26. https://doi.org/10.1016/j.jplph.2017.06.010

Krylov, D., Mikhailenko, I., & Vinson, C. (1994). A thermodynamic scale for leucine zipper stability

and dimerization specificity: e and g interhelical interactions. *The EMBO Journal*, *13*(12), 2849. https://doi.org/10.1002/J.1460-2075.1994.TB06579.X

Kumar, S., Stecher, G., Li, M., Knyaz, C., & Tamura, K. (2018). MEGA X: Molecular Evolutionary Genetics Analysis across Computing Platforms. *Molecular Biology and Evolution*, *35*(6), 1547–1549. https://doi.org/10.1093/MOLBEV/MSY096

Lee, R. E. (2018). Phycology. *Phycology*. https://doi.org/10.1017/9781316407219

Lin, M., & Guo, J. T. (2019). New insights into protein–DNA binding specificity from hydrogen bond based comparative study. *Nucleic Acids Research*, *47*(21), 11103–11113. https://doi.org/10.1093/NAR/GKZ963

Mann, M., Serif, M., Wrobel, T., Eisenhut, M., Madhuri, S., Flachbart, S., Weber, A. P. M., Lepetit, B., Wilhelm, C., & Kroth, P. G. (2020). The Aureochrome Photoreceptor PtAUREO1a Is a Highly Effective Blue Light Switch in Diatoms. *IScience*, *23*(11), 101730. https://doi.org/10.1016/J.ISCI.2020.101730

Matiiv, A. B., & Chekunova, E. M. (2018). Aureochromes – Blue Light Receptors. *Biochemistry (Moscow)*, *83*(6), 662–673. https://doi.org/10.1134/S0006297918060044

Mitra, D., Yang, X., & Moffat, K. (2012). Crystal structures of aureochrome1 LOV suggest new design strategies for optogenetics. *Structure*. https://doi.org/10.1016/j.str.2012.02.016

Negre, C. F. A., Morzan, U. N., Hendrickson, H. P., Pal, R., Lisi, G. P., Patrick Loria, J., Rivalta, I., Ho, J., & Batista, V. S. (2018). Eigenvector centrality for characterization of protein allosteric pathways. *Proceedings of the National Academy of Sciences of the United States of America*, *115*(52), E12201–E12208. https://doi.org/10.1073/PNAS.1810452115

Pettersen, E. F., Goddard, T. D., Huang, C. C., Couch, G. S., Greenblatt, D. M., Meng, E. C., & Ferrin, T. E. (2004). UCSF Chimera—A visualization system for exploratory research and analysis. *Journal of Computational Chemistry*, *25*(13), 1605–1612. https://doi.org/10.1002/JCC.20084

Podust, L. M., Krezel, A. M., & Kim, Y. (2001). Crystal structure of the CCAAT box/enhancer-binding protein beta activating transcription factor-4 basic leucine zipper heterodimer in the absence of DNA. *The Journal of Biological Chemistry*, *276*(1), 505–513. https://doi.org/10.1074/JBC.M005594200

Pogenberg, V., Consani Textor, L., Vanhille, L., Holton, S. J., Sieweke, M. H., & Wilmanns, M. (2014). Design of a bZip Transcription Factor with Homo/Heterodimer-Induced DNA-Binding Preference. *Structure*, *22*(3), 466–477. https://doi.org/10.1016/j.str.2013.12.017

Porte, D., Oertel-Buchheit, P., John, M., Granger-Schnarr, M., & Schnarr, M. (1997). DNA binding and transactivation properties of Fos variants with homodimerization capacity. *Nucleic Acids Research*, *25*(15), 3026–3033. https://doi.org/10.1093/NAR/25.15.3026

Pronk, S., Páll, S., Schulz, R., Larsson, P., Bjelkmar, P., Apostolov, R., Shirts, M. R., Smith, J. C., Kasson, P. M., Van Der Spoel, D., Hess, B., & Lindahl, E. (2013). GROMACS 4.5: a high-throughput and highly parallel open source molecular simulation toolkit. *Bioinformatics*, *29*(7), 845–854. https://doi.org/10.1093/BIOINFORMATICS/BTT055

Rayko, E., Maumus, F., Maheswari, U., Jabbari, K., & Bowler, C. (2010). Transcription factor families inferred from genome sequences of photosynthetic stramenopiles. *The New Phytologist*, *188*(1), 52–66. https://doi.org/10.1111/J.1469-8137.2010.03371.X

Rodríguez-Martínez, J. A., Reinke, A. W., Bhimsaria, D., Keating, A. E., & Ansari, A. Z. (2017). Combinatorial bZIP dimers display complex DNA-binding specificity landscapes. *ELife*, *6*.

https://doi.org/10.7554/eLife.19272

Schumacher, M. A., Goodman, R. H., & Brennan, R. G. (2000). *The Structure of a CREB bZIPSomatostatin CRE Complex Reveals the Basis for Selective Dimerization and Divalent Cation-enhanced DNA Binding**. https://doi.org/10.1074/jbc.M007293200

Sievers, F., Wilm, A., Dineen, D., Gibson, T. J., Karplus, K., Li, W., Lopez, R., McWilliam, H., Remmert, M., Söding, J., Thompson, J. D., & Higgins, D. G. (2011). Fast, scalable generation of high-quality protein multiple sequence alignments using Clustal Omega. *Molecular Systems Biology*, *7*(1), 539. https://doi.org/10.1038/MSB.2011.75

Sinden, R. R. (1994). DNA–Protein Interactions. *DNA Structure and Function*, 287–325. https://doi.org/10.1016/B978-0-08-057173-7.50013-4

Takahashi, F., Yamagata, D., Ishikawa, M., Fukamatsu, Y., Ogura, Y., Kasahara, M., Kiyosue, T., Kikuyama, M., Wada, M., & Kataoka, H. (2007). AUREOCHROME, a photoreceptor required for photomorphogenesis in stramenopiles. *Proceedings of the National Academy of Sciences*, *104*(49), 19625–19630. https://doi.org/10.1073/pnas.0707692104

Tuszynska, I., Magnus, M., Jonak, K., Dawson, W., & Bujnicki, J. M. (2015). NPDock: a web server for protein–nucleic acid docking. *Nucleic Acids Research*, *43*(Web Server issue), W425. https://doi.org/10.1093/NAR/GKV493

Van Der Spoel, D., Lindahl, E., Hess, B., Groenhof, G., Mark, A. E., & Berendsen, H. J. C. (2005). GROMACS: Fast, flexible, and free. *Journal of Computational Chemistry*, *26*(16), 1701–1718. https://doi.org/10.1002/JCC.20291

Vinson, C., Myakishev, M., Acharya, A., Mir, A. A., Moll, J. R., & Bonovich, M. (2002). Classification of Human B-ZIP Proteins Based on Dimerization Properties. *Molecular and Cellular Biology*, *22*(18), 6321–6335. https://doi.org/10.1128/MCB.22.18.6321-6335.2002

Vinson, C. R., Hai, T., & Boyd, S. M. (1993). Dimerization specificity of the leucine zipper-containing bZIP motif on DNA binding: Prediction and rational design. *Genes and Development*, *7*(6), 1047–1058. https://doi.org/10.1101/gad.7.6.1047

Wang, Y., Zhang, Y., Zhou, R., Dossa, K., Yu, J., Li, D., Liu, A., Mmadi, M. A., Zhang, X., & You, J. (2018). Identification and characterization of the bZIP transcription factor family and its expression in response to abiotic stresses in sesame. *PLOS ONE*, *13*(7), e0200850. https://doi.org/10.1371/journal.pone.0200850

Waterhouse, A., Bertoni, M., Bienert, S., Studer, G., Tauriello, G., Gumienny, R., Heer, F. T., De Beer, T. A. P., Rempfer, C., Bordoli, L., Lepore, R., & Schwede, T. (2018). SWISS-MODEL: homology modelling of protein structures and complexes. *Nucleic Acids Research*, *46*(W1), W296–W303. https://doi.org/10.1093/NAR/GKY427

Figure 1

a

| | | DNA binding domain | | |

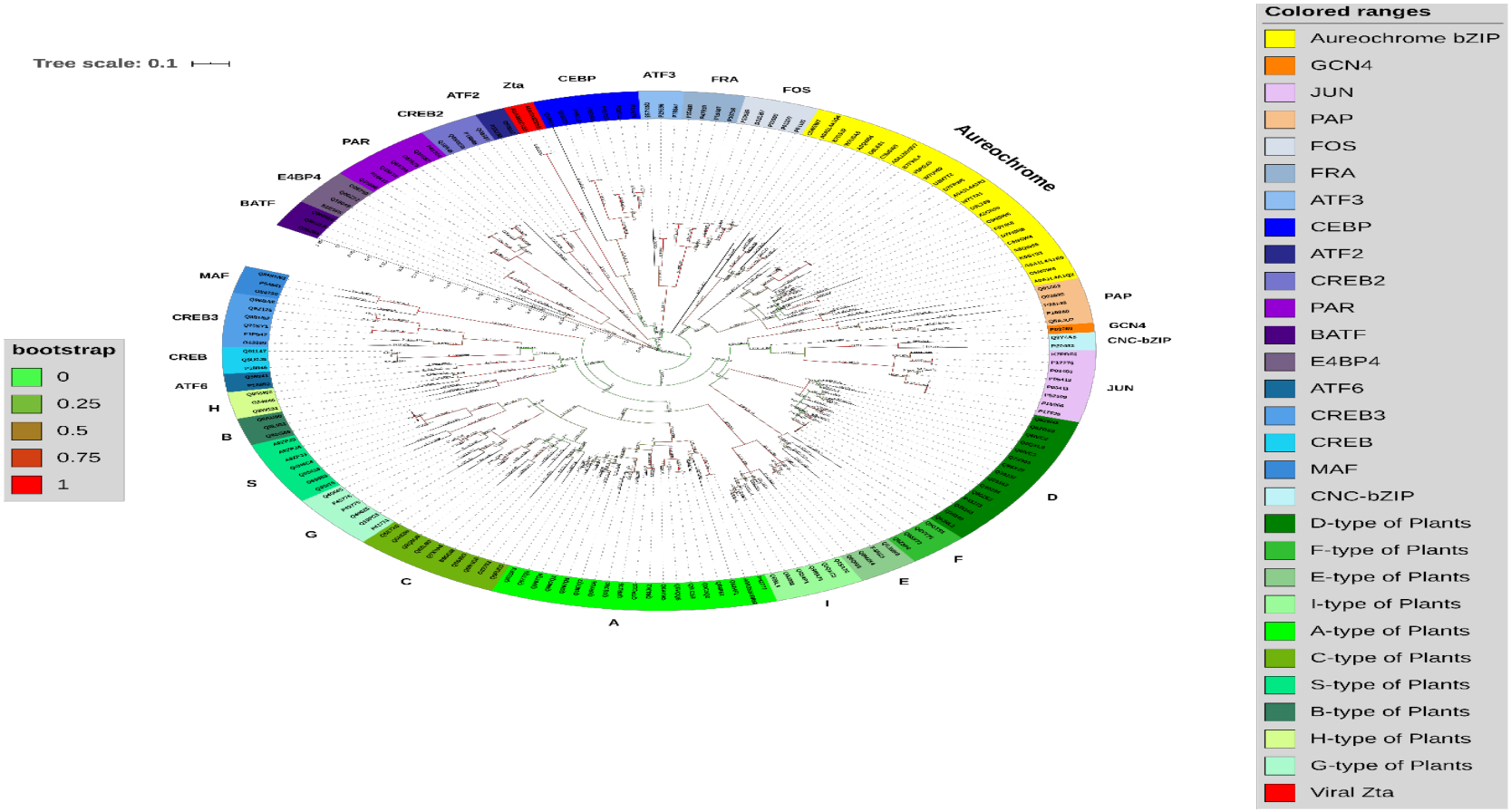
Tree scale: 0.1
bootstrap
0
0.25
0.5
0.75
1
Aureochrome
ATF3
FRA
FOS
CEBP
Zta
ATF2
CREB2
PAR
E4BP4
BATF
MAF
CREB3
CREB
ATF6
H
B
S
G
C
A
I
E
F
D
JUN
CNC-bZIP
GCN4
PAP
Colored ranges
Aureochrome bZIP
GCN4
JUN
PAP
FOS
FRA
ATF3
CEBP
ATF2
CREB2
PAR
BATF
E4BP4
ATF6
CREB3
CREB
MAF
CNC-bZIP
D-type of Plants
F-type of Plants
E-type of Plants
I-type of Plants
A-type of Plants
C-type of Plants
S-type of Plants
B-type of Plants
H-type of Plants
G-type of Plants
Viral Zta

Figure 2

Figure 3

a

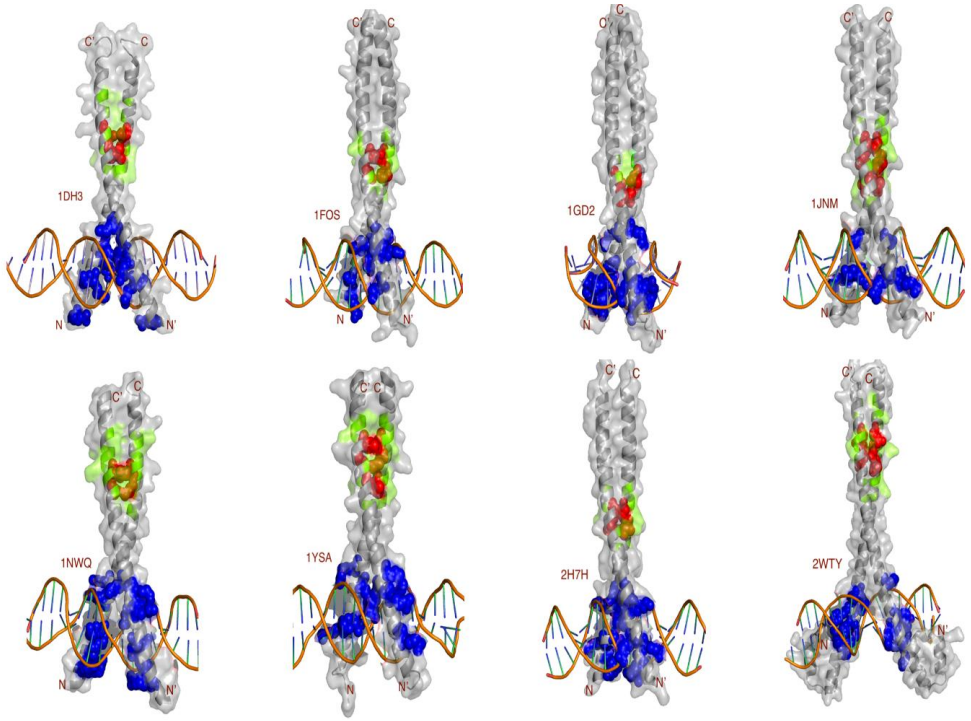

b

```
                                gabcdefgabcdefgabcdefgabcdefgabcd
PAP GD2     SSKRKAQNRAAQRAFRKRKEDHLKALETQVVTLKELHSSTTLENDQLRQKVRQLEEEL
C-FOS       RRIRRERNKMAAAKSRNRRRELTDTLQAETDQLEDEKSALQTEIANLLKEKEKLEFIL
1FOS
C-JUN       AERKRMRNRIAASKSRKRKLERIARLEEKVKTLKAQNSELASTANMLREQVAQLKQKV
1FOS
GCN4        AALKRARNTEAARRSRARKLQRMKQLEDKVEELLSKNYHLENEVARLKKLVGER----
1YSA
ViralJUN    AERKRMRNRIAASKSRKRKLERIARLEEKVKTLKAQNSELASTANMLREQVAQLKQKV
2H7H
CEBP        YRVRRERNNIAVRKSRDKAKQRNVETQQKVLELTSDNDRLRKRVEQLSRELDTLRG--
1NWQ
CREB        REVRLMKNREAARESRRKKKEYVKSLENRVAVLENQNKTLIEELKALKDLYSHK----
1DH3
C-JUN       AERKRMRNRIAASKSRKRKLERIARLEEKVKTLKAQNSELASTANMLREQVAQLKQKV
1JNM
MAFB        QKRRTLKNRGYAQSCRYKRVQQKHHLENEKTQLIQQVEQLKQEVSRLARERDAYKVKS
2WTY
EsAureo1    RIERRERNREHAKRSRVRKKFLLDSLQRSVDAIQAENESLKGSIVGSLGERGREL---
EsAureo2    AKKRRERNRVLARRTRLRKKFFFQSLQQQVARLQRENERLKGIVTTRCPDSVGEIL--
EsAureo3    RLDRRERNREHAKRSRVRKKFLLESLQKSVTSLQEENEKLRGAIRSNLGPEEAKEL--
EsAureo4    KLERRERNREHAKRSRIRKKFMLECLQEQLLAMRKQNLALRQVVKEHMPDEASTV---
```

Heptad-1 Heptad-2 Heptad-3 Heptad-4

Figure 4

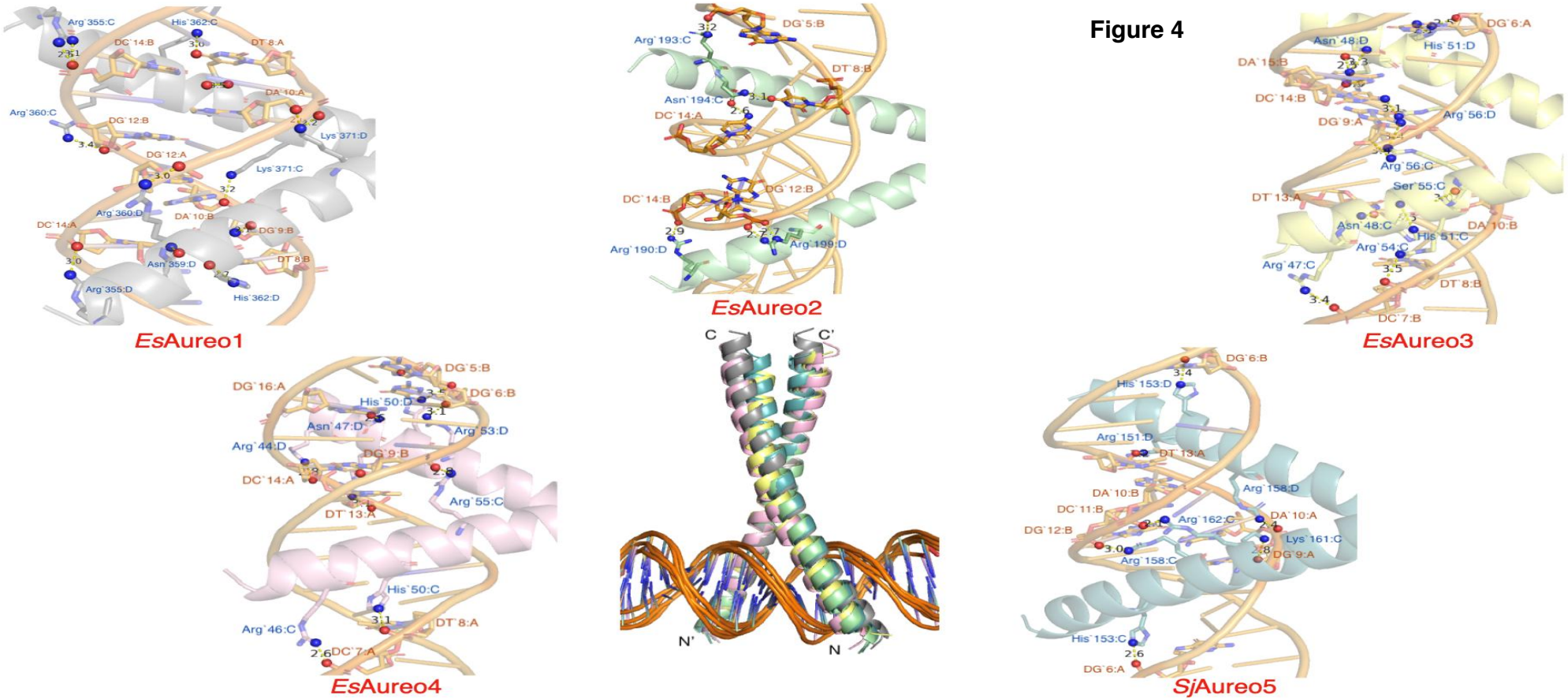
Arg`355:C
His`362:C
DC`14:B
DT`8:A
DA`10:A
Arg`360:C
DG`12:B
Lys`371:D
DG`12:A
Lys`371:C
Arg`360:D
DA`10:B
DC`14:A
DG`9:B
Asn`359:D
DT`8:B
Arg`355:D
His`362:D
EsAureo1
DG`5:B
Arg`193:C
DT`8:B
Asn`194:C
DC`14:A
DG`12:B
DC`14:B
Arg`190:D
Arg`199:D
EsAureo2
C
C'
N'
N
DG`16:A
DG`5:B
DG`6:B
His`50:D
Asn`47:D
Arg`53:D
Arg`44:D
DG`9:B
DC`14:A
Arg`55:C
DT`13:A
His`50:C
Arg`46:C
DT`8:A
DC`7:A
EsAureo4
Asn`48:D
His`51:D
DG`6:A
DA`15:B
DC`14:B
DG`9:A
Arg`56:D
Arg`56:C
Ser`55:C
DT`13:A
Asn`48:C
DA`10:B
His`51:C
Arg`54:C
Arg`47:C
DT`8:B
DC`7:B
EsAureo3
DG`6:B
His`153:D
Arg`151:D
DT`13:A
Arg`158:D
DA`10:B
DC`11:B
Arg`162:C
DA`10:A
DG`12:B
Lys`161:C
Arg`158:C
DG`9:A
His`153:C
DG`6:A
SjAureo5

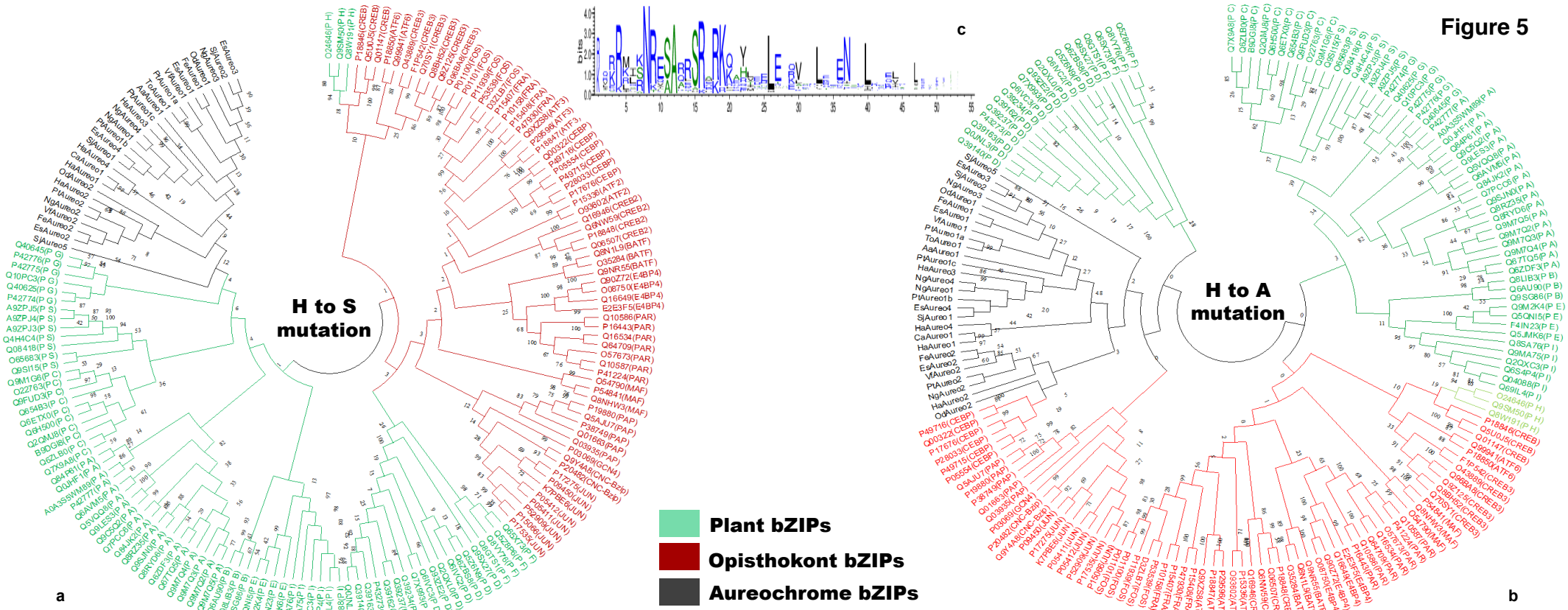
Figure 5
H to S mutation
H to A mutation
a
b
c
bits
Plant bZIPs
Opisthokont bZIPs
Aureochrome bZIPs

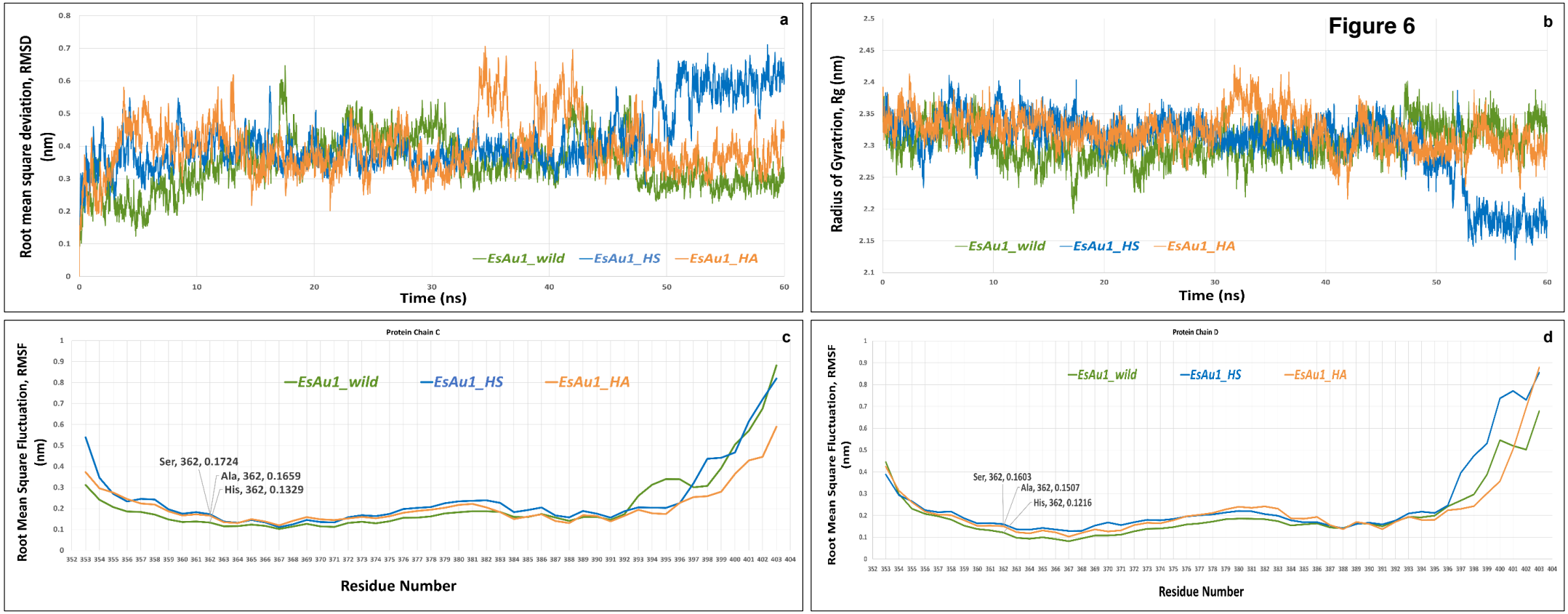
Figure 6
a
Root mean square deviation, RMSD (nm)
Time (ns)
EsAu1_wild
EsAu1_HS
EsAu1_HA
b
Radius of Gyratrion, Rg (nm)
Time (ns)
EsAu1_wild
EsAu1_HS
EsAu1_HA
c
Protein Chain C
Root Mean Square Fluctuation, RMSF (nm)
Residue Number
EsAu1_wild
EsAu1_HS
EsAu1_HA
Ser, 362, 0.1724
Ala, 362, 0.1659
His, 362, 0.1329
d
Protein Chain D
Root Mean Square Fluctuation, RMSF (nm)
Residue Number
EsAu1_wild
EsAu1_HS
EsAu1_HA
Ser, 362, 0.1603
Ala, 362, 0.1507
His, 362, 0.1216

Figure 7

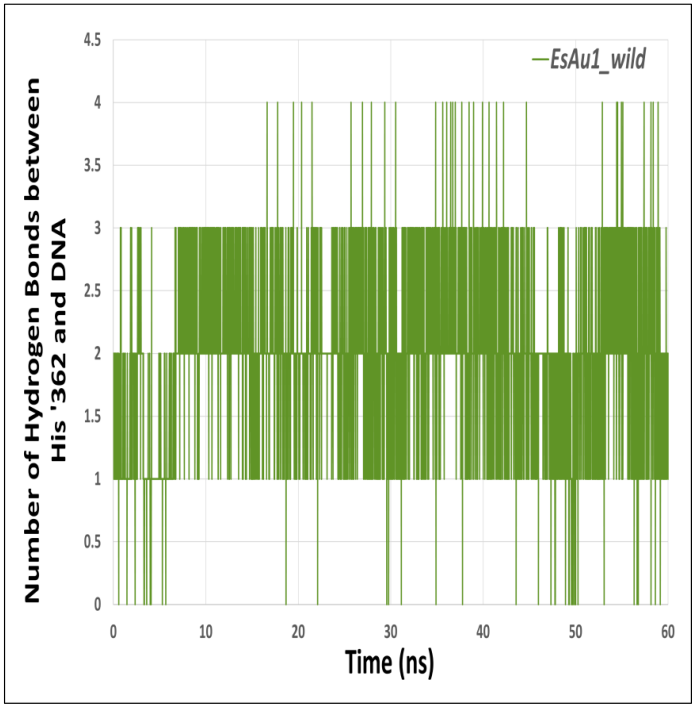
EsAu1_wild
Number of Hydrogen Bonds between His '362 and DNA
Time (ns)
0
0.5
1
1.5
2
2.5
3
3.5
4
4.5
0
10
20
30
40
50
60

a

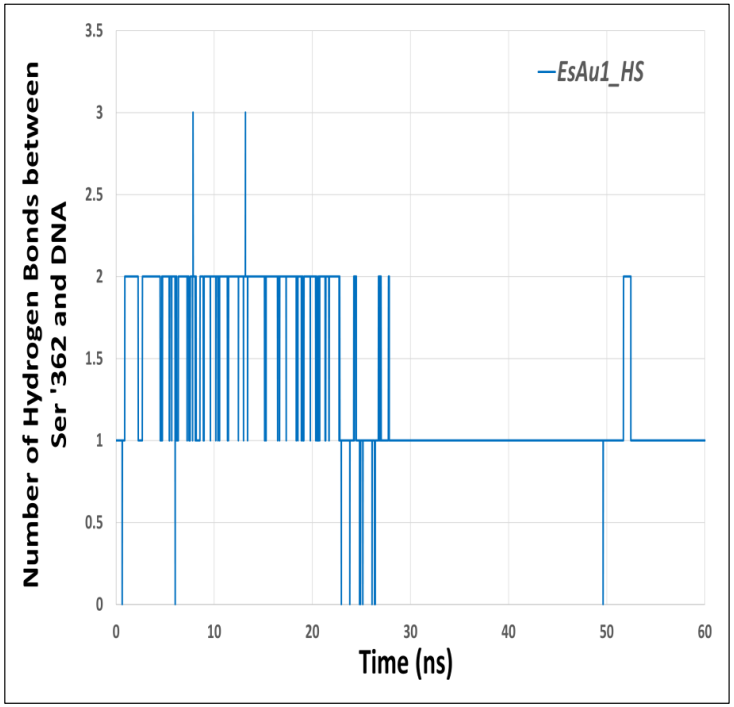
EsAu1_HS
Number of Hydrogen Bonds between Ser '362 and DNA
Time (ns)
0
0.5
1
1.5
2
2.5
3
3.5
0
10
20
30
40
50
60

b

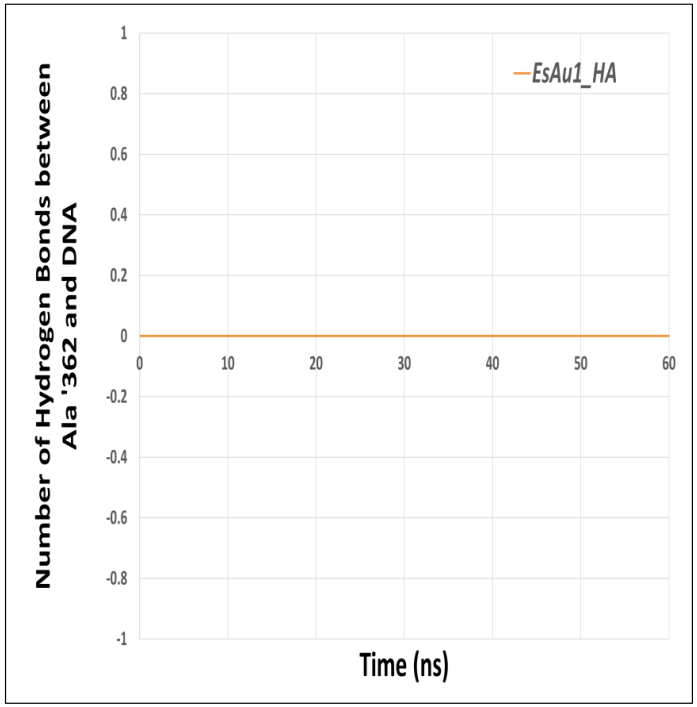
EsAu1_HA
Number of Hydrogen Bonds between Ala '362 and DNA
Time (ns)
1
0.8
0.6
0.4
0.2
0
-0.2
-0.4
-0.6
-0.8
-1
0
10
20
30
40
50
60

c

Figure 8

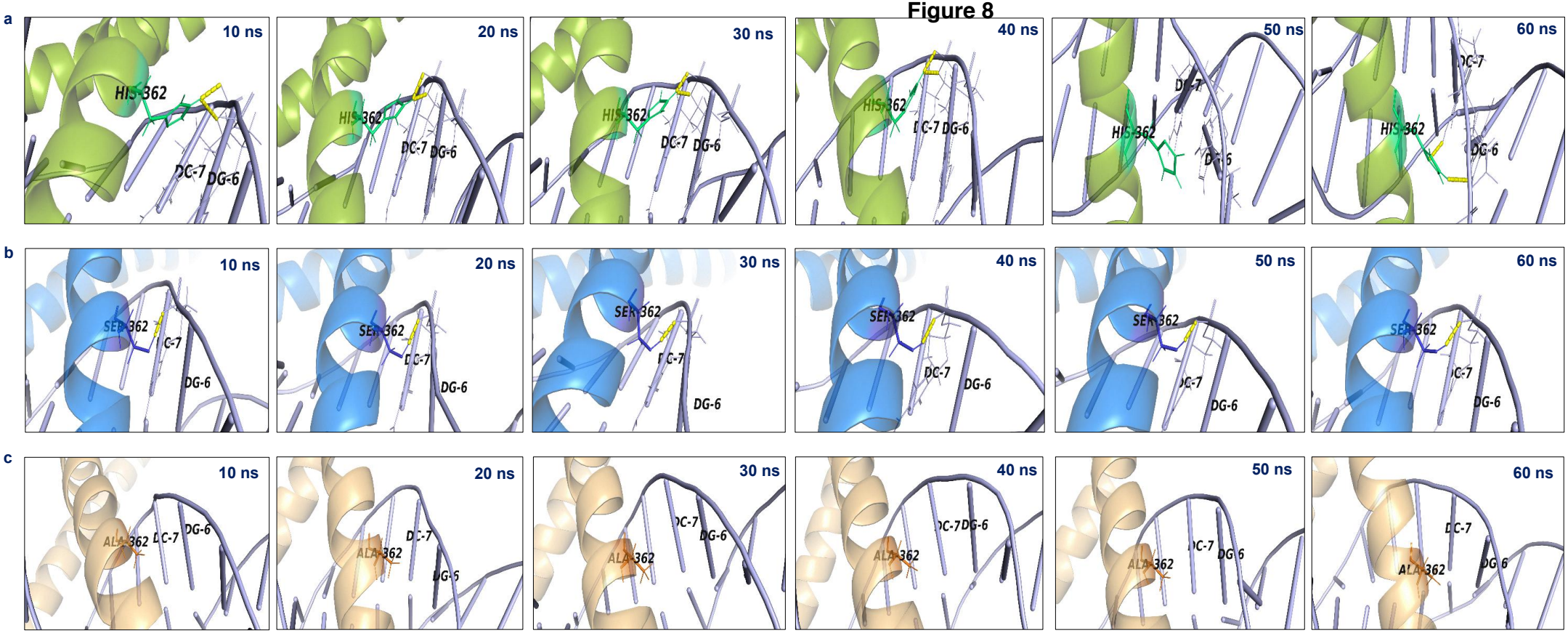
a
10 ns
20 ns
30 ns
40 ns
50 ns
60 ns
HIS-362
DC-7
DG-6
b
SER-362
c
ALA-362

Figure 9

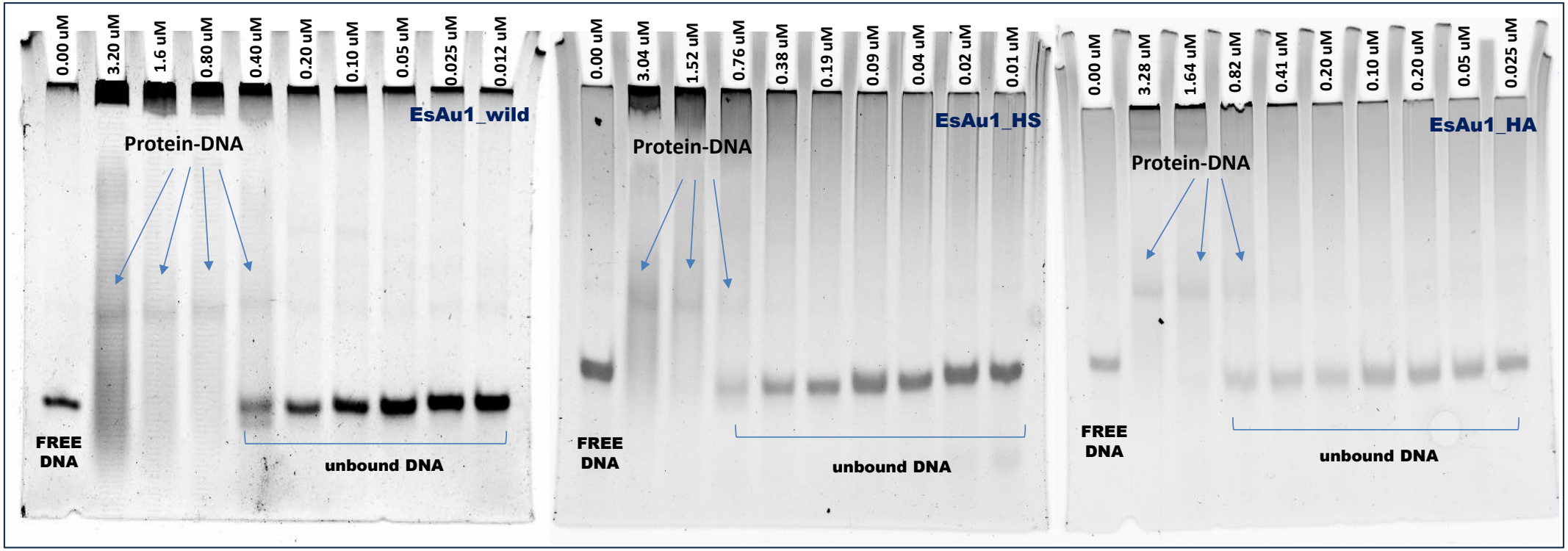
0.00 uM
3.20 uM
1.6 uM
0.80 uM
0.40 uM
0.20 uM
0.10 uM
0.05 uM
0.025 uM
0.012 uM
EsAu1_wild
Protein-DNA
FREE DNA
unbound DNA
0.00 uM
3.04 uM
1.52 uM
0.76 uM
0.38 uM
0.19 uM
0.09 uM
0.04 uM
0.02 uM
0.01 uM
EsAu1_HS
Protein-DNA
FREE DNA
unbound DNA
0.00 uM
3.28 uM
1.64 uM
0.82 uM
0.41 uM
0.20 uM
0.10 uM
0.20 uM
0.05 uM
0.025 uM
EsAu1_HA
Protein-DNA
FREE DNA
unbound DNA

a b c

Figure 10

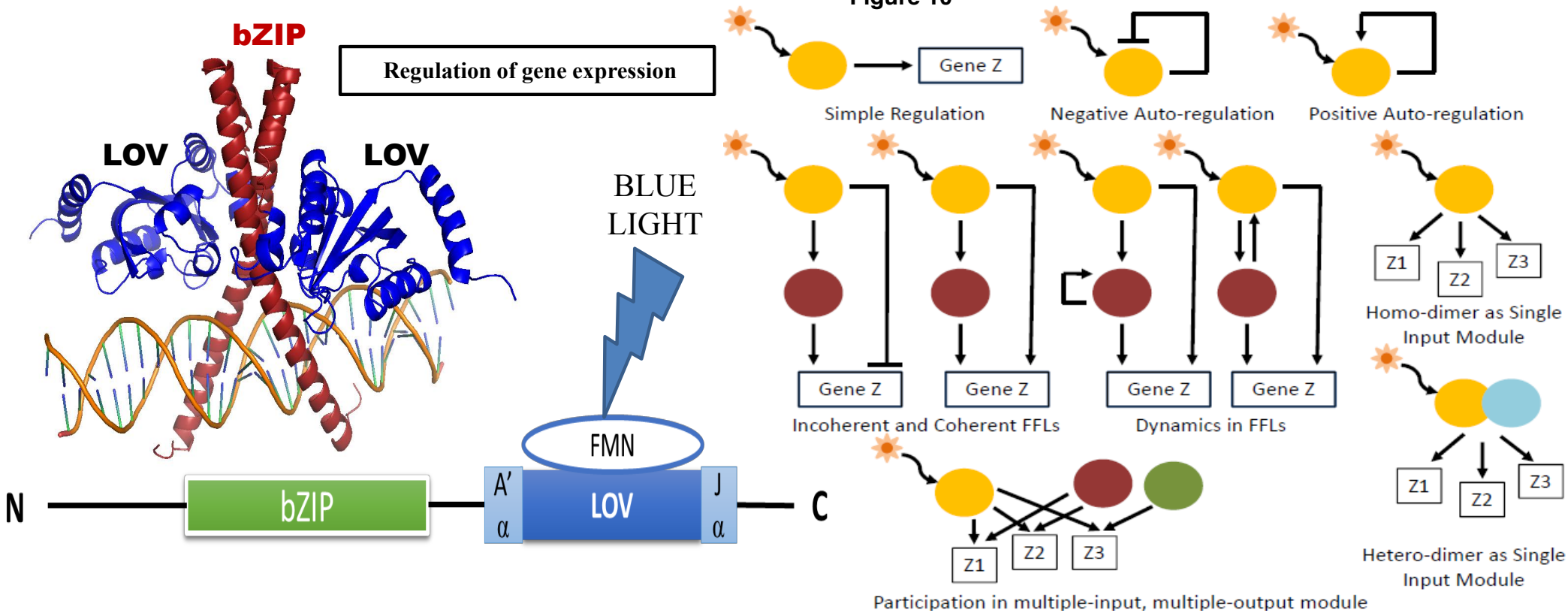
bZIP
LOV
LOV
Regulation of gene expression
BLUE LIGHT
FMN
N
bZIP
A'
α
LOV
J
α
C
Gene Z
Simple Regulation
Negative Auto-regulation
Positive Auto-regulation
Gene Z
Gene Z
Gene Z
Gene Z
Incoherent and Coherent FFLs
Dynamics in FFLs
Z1
Z2
Z3
Homo-dimer as Single Input Module
Z1
Z2
Z3
Hetero-dimer as Single Input Module
Z1
Z2
Z3
Participation in multiple-input, multiple-output module